

Dirty black hole binaries as probe of dark matter halos

@ Dark Matter and Stars, 3 May 2023

In collaboration with

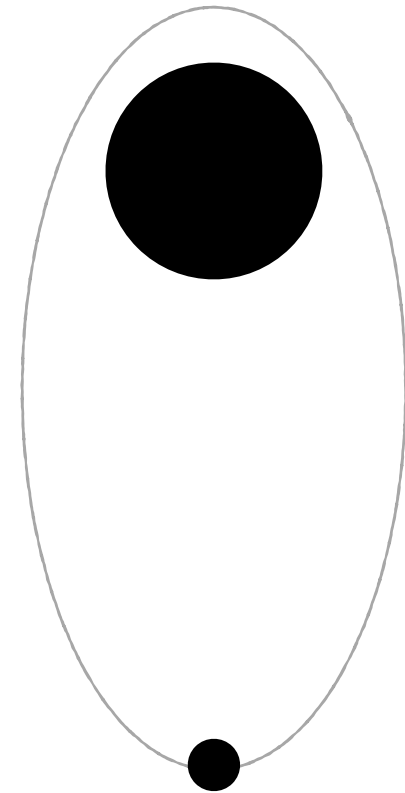
V. Cardoso, F. Duque, K. Destounis, R. Panoso, E. Figueiredo



Andrea Maselli

Milestones

- *Asymmetric binaries as natural (golden) laboratories to test fundamental physics*
 - *top-notch to study the (generic) environment in which binaries evolve*
- *How do we build a relativistic BH solutions embedded within a core of matter?*
 - *Are astrophysical observables affected by the non-vacuum background?*
 - *Which are the best observables to capture the properties of the environment?*



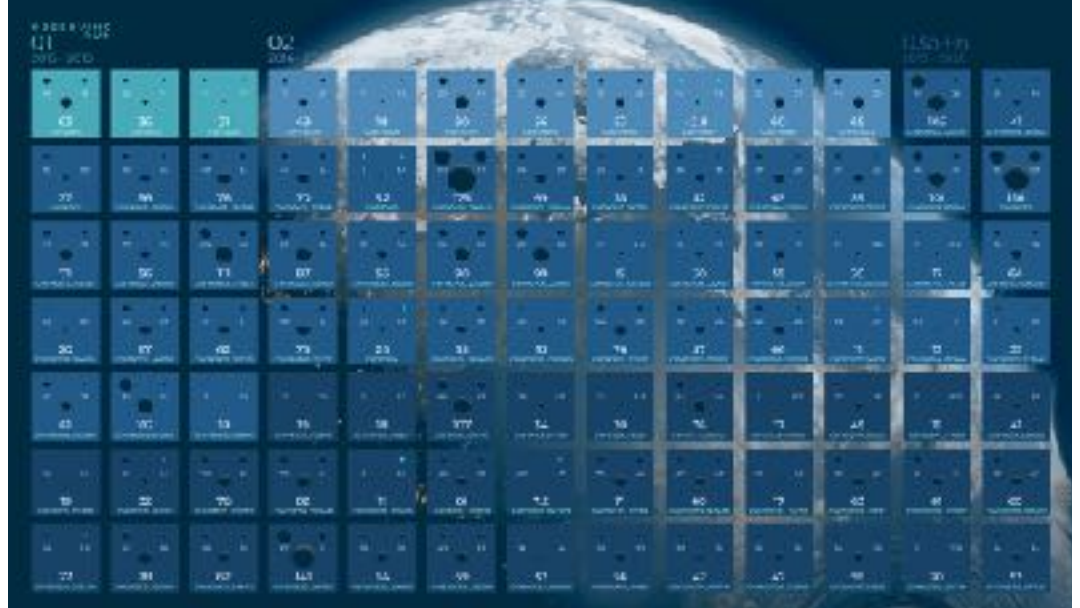
Why asymmetric binaries?

90+ events observed so far from LVK, spanning a relatively small interval of mass ratios $q \sim 1 : 30$

- *3G detectors are expected to beat down such value by several orders of magnitudes*

$$q \sim 10^{-6} - 10^{-7}$$

- *dynamics mostly dictated by **q**, with the duration of the inspiral & number of cycles growing as q decreases*



LVK GWTC 3 2111.03605

A discovery potential in 3 moves

- 1 *Slow inspiral phase which could allow to continuously observe AB for very long periods, from months to years*
- 2 *dynamical evolutions with an uncommon richness, with resonances, large eccentricities and off-equatorial orbits, etc.*
- 3 *astro-fundamental physics setups*

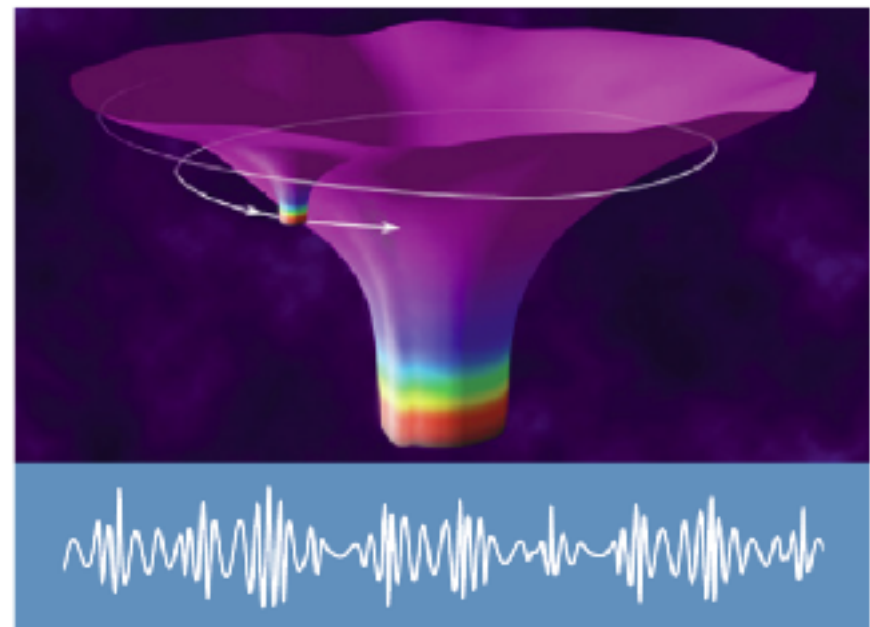
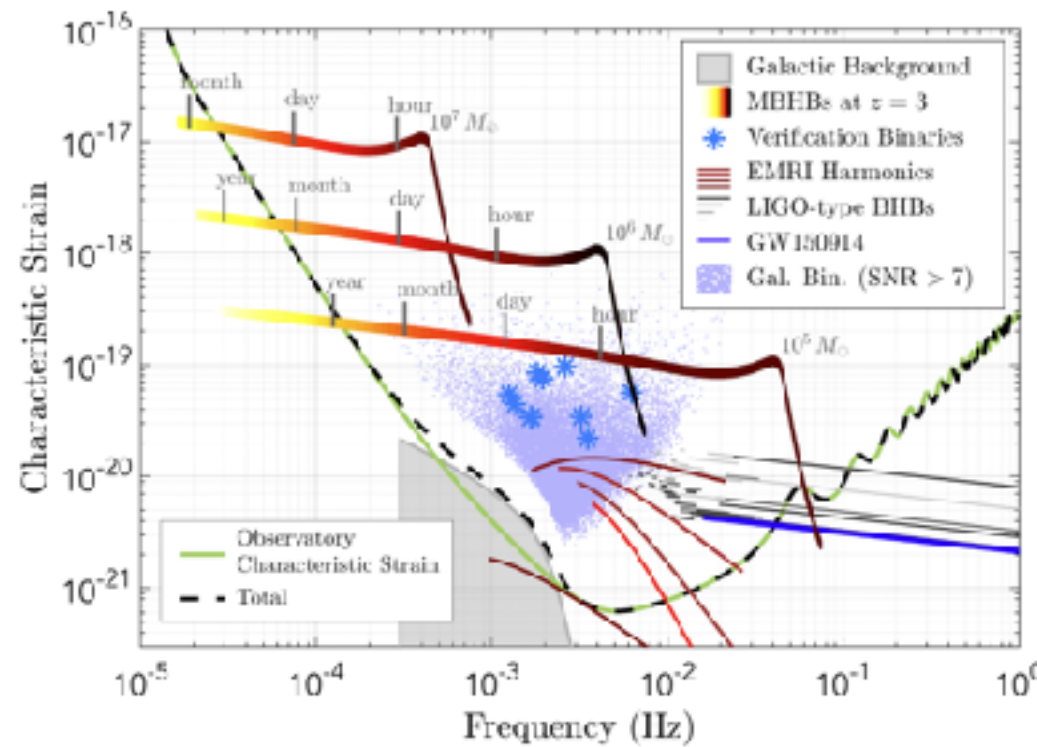
Extreme Mass Ratio Inspirals

Binary systems with a stellar-mass body inspiralling into a massive black hole

- Primary with $M \sim (10^4 - 10^8)M_\odot$
- Secondary such that the mass ratio

$$q = m_p/M \sim (10^{-6} - 10^{-3})$$

- Key point of theoretical description

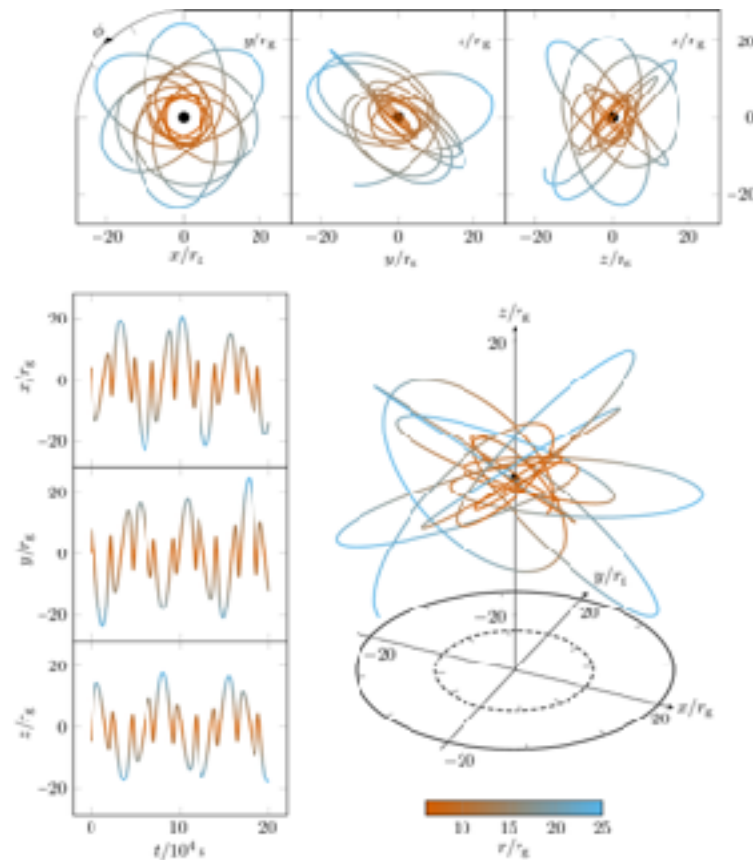


- Emit GWs in the mHz band, golden targets for LISA

EMRI in nuce

1 2

EMRIs provide a rich phenomenology, due to their orbital features



- Non equatorial orbits
- Eccentric motion
- Resonances
- Complete $\sim (10^4 - 10^5)$ cycles before the plunge

bless and disguise

Tracking EMRIs for $O(\text{year})$ requires accurate templates

Berry +, Astro2020 1903.03686 (2019)

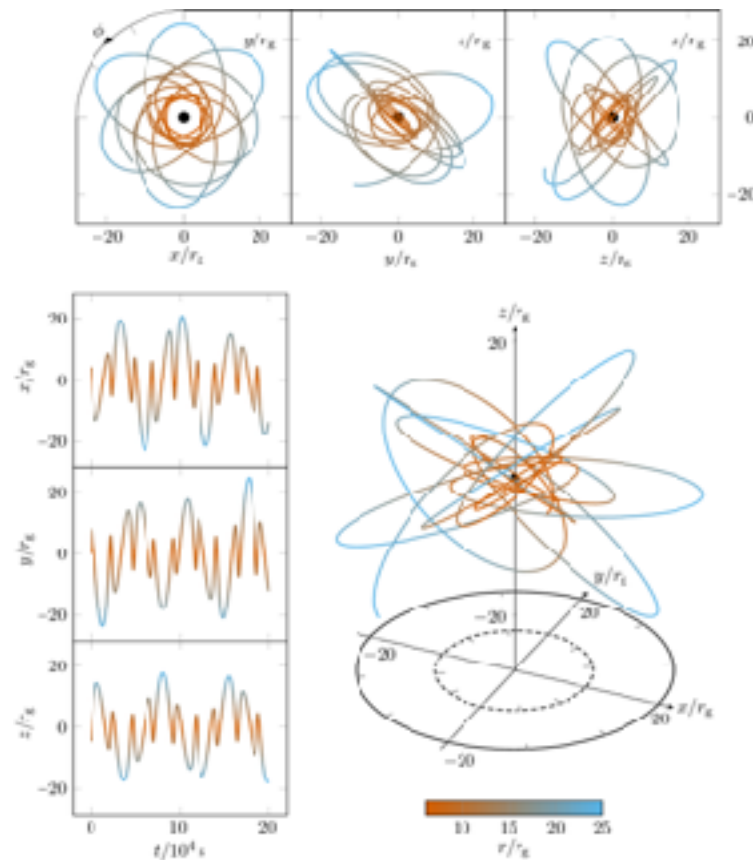
Very appealing to test fundamental & astro-physics

Precise space-time map and accurate binary parameters

EMRI in nuce

1 2

EMRIs provide a rich phenomenology, due to their orbital features



- Non equatorial orbits
- Eccentric motion
- Resonances
- Complete $\sim (10^4 - 10^5)$ cycles before the plunge

bless and disguise

Tracking EMRIs for $O(\text{year})$ requires accurate templates

Berry +, Astro2020 1903.03686 (2019)

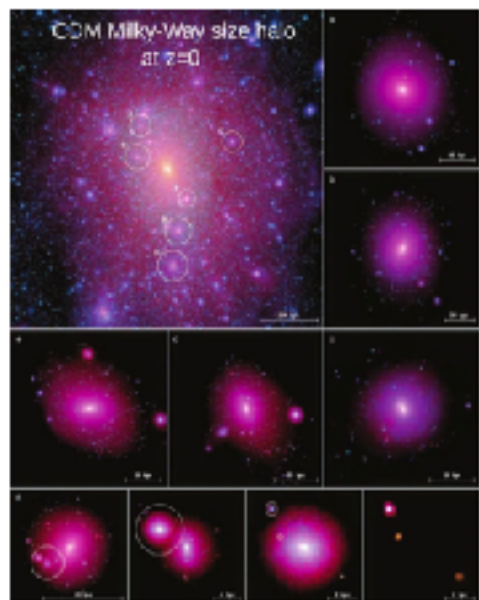
what are the features of the astrophysical environments in which binary systems evolve?

Dirty & asymmetric BBHs

GW sources evolve embedded in a variety of gas/matter contents/fields, which may leave detectable imprints on GW

3

- *Can we infer properties on the environment in which binaries evolve?*
- *Are vacuum waveform models safe?*



V. Springel et al., Mon. Not. Roy. Astron. 391 (2008)



G. Bertone et al., Nature 562, 7725 (2008)

MBH and inspirals evolve in DM-rich environment, within galaxies

IMIR/EMRI can assemble in accretion disks



particle physics laboratories

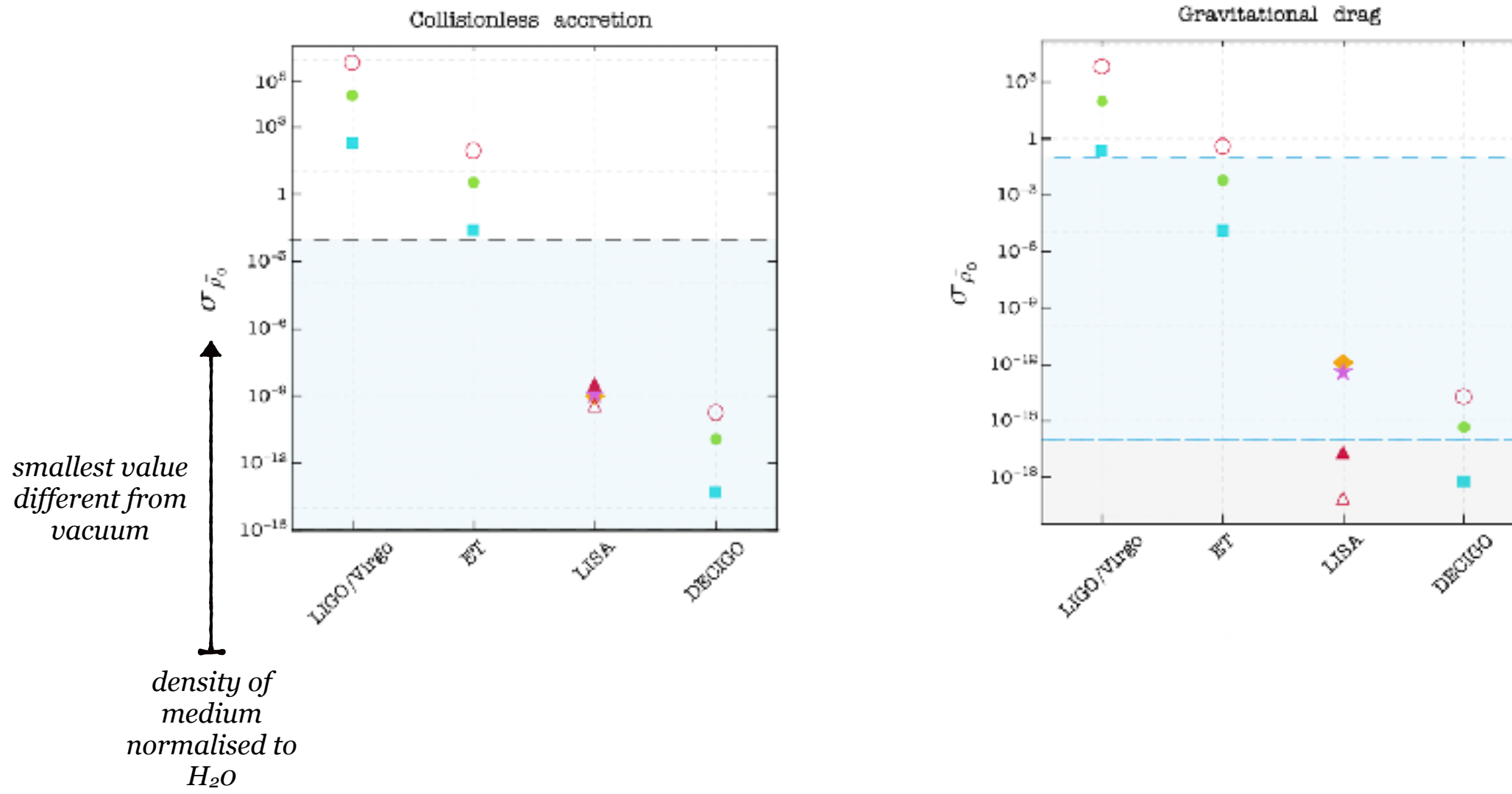
Why EMRIs?

Constraints on the environment's density from different effects/sources/detectors

V. Cardoso & A. M., *A&A* 644, A147 (2020)

Useful (extrapolated) lessons from comparable mass binaries

-  *environmental effects typically contribute at low frequencies*



Why EMRIs?

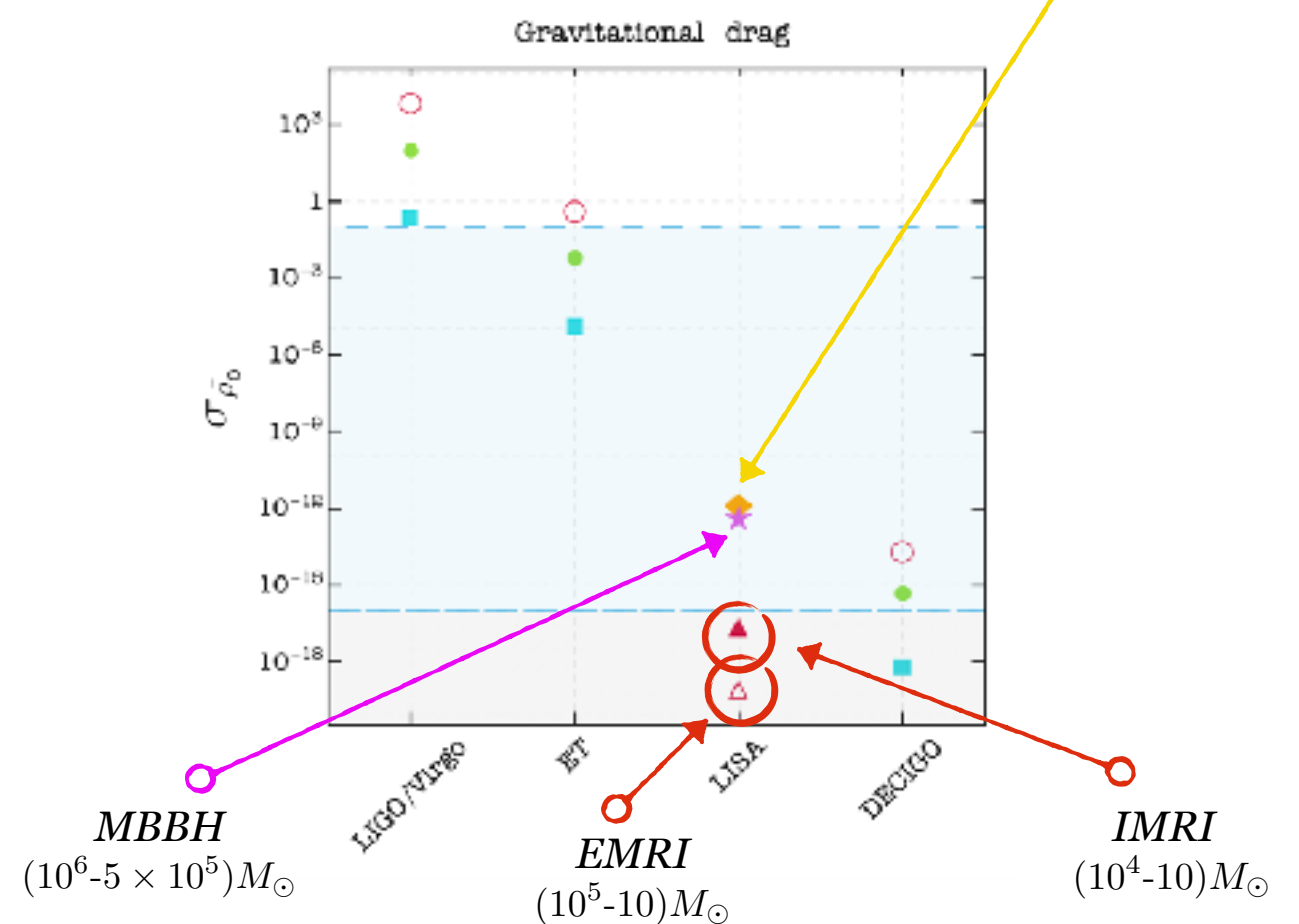
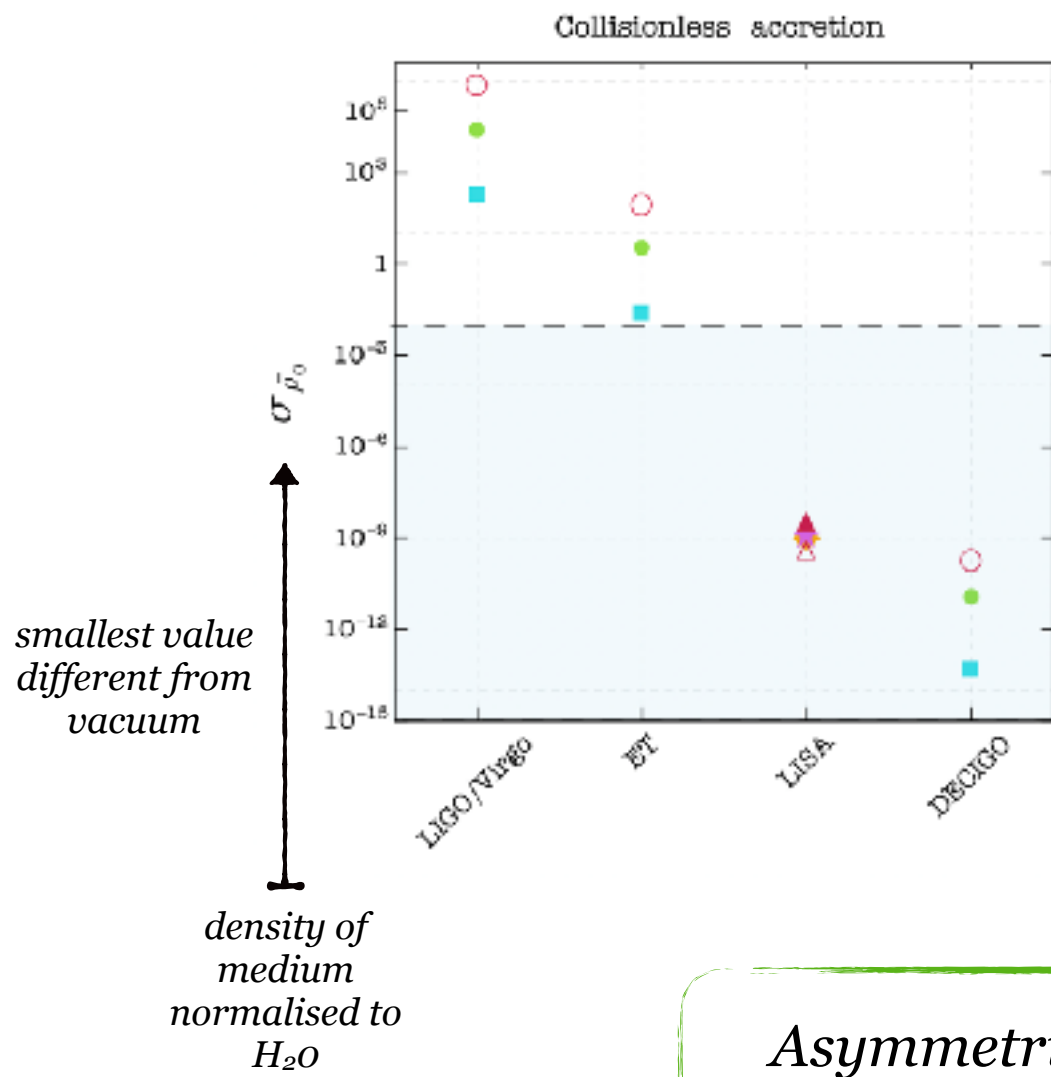
Constraints on the *environment's density* from different effects/sources/detectors

V. Cardoso & A. M., A&A 644, A147 (2020)

Useful (extrapolated) lessons from comparable mass binaries

- environmental effects typically contribute at low frequencies

$(10^4-5 \times 10^3) M_\odot$
IBBH



Asymmetric binaries work (really) well

What goes into an EMRI?

Using EMRI observations for precision astrophysics is a complex task

- The **Self-Force** program in (**vacuum** GR) is @ work for more than two decades for second order waveforms

Barack & Pound, Rep. Prog. Phys. 82 016904 (2018)

- Complexity of calculations beyond standard vacuum BBH grows very (very fast)

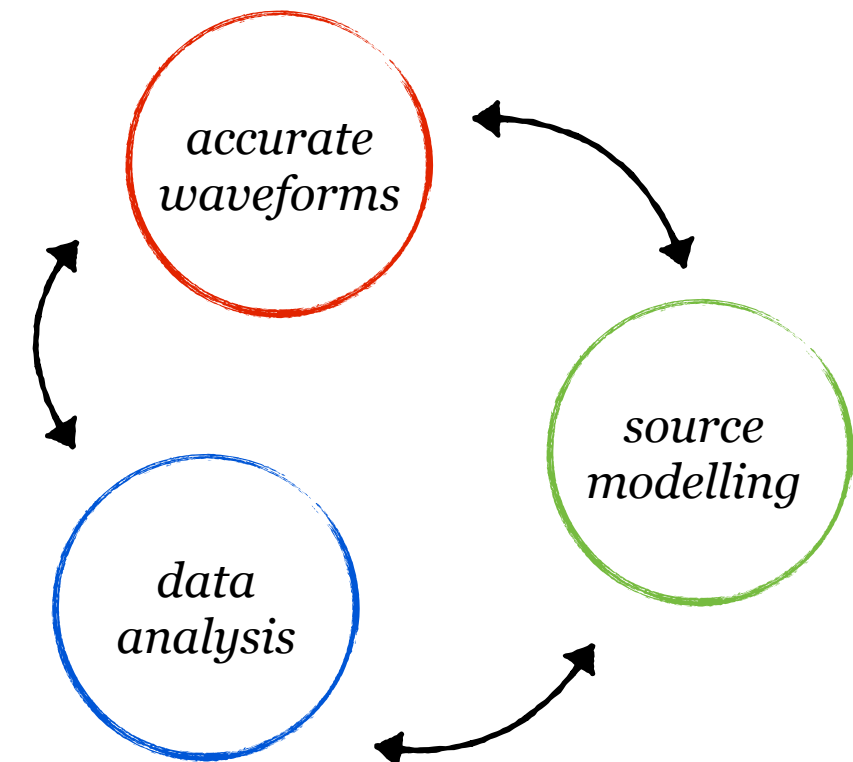
- Couplings with extra fields

*A.M. et al. Nature Astronomy 6, 4 464-470 (2022)
V. Cardoso et al., Phys. Rev. D 105, L061501 (2022)*

- Even the background solutions are poorly characterised (spin?)

- Generation of (fast) waveform models

Katz +, PRD 104 064047 (2021)



EMRI in vacuum

How do we study EMRI in vacuum (GR)?

- *The asymmetric character introduces a natural parameter to study the problem in perturbation theory $q = m_p/M \ll 1$*

$$g_{\alpha\beta} = g_{\alpha\beta}^{(0)} + h_{\alpha\beta}$$
$$G_{\mu\nu} = T_{\mu\nu}^p = 8\pi m_p \int \frac{\delta^{(4)}(x - y_p(\lambda))}{\sqrt{-g}} \frac{dy_p^\alpha}{d\lambda} \frac{dy_p^\beta}{d\lambda} d\lambda$$

leading 
adiabatic

*Regge-Wheeler-Zerilli
(Schwarzschild
background)*

*Teukolsky
(Kerr
background)*

- *The solution determines the phase evolution*

$$\phi(t) = \phi_{\text{diss}-1} + \dots$$

adiabatic *first post-adiabatic*

 $\mathcal{O}(1/q)$  $\mathcal{O}(1)$

EMRI in vacuum

How do we study EMRI in vacuum (GR)?

- The asymmetric character introduces a natural parameter to study the problem in perturbation theory $q = m_p/M \ll 1$

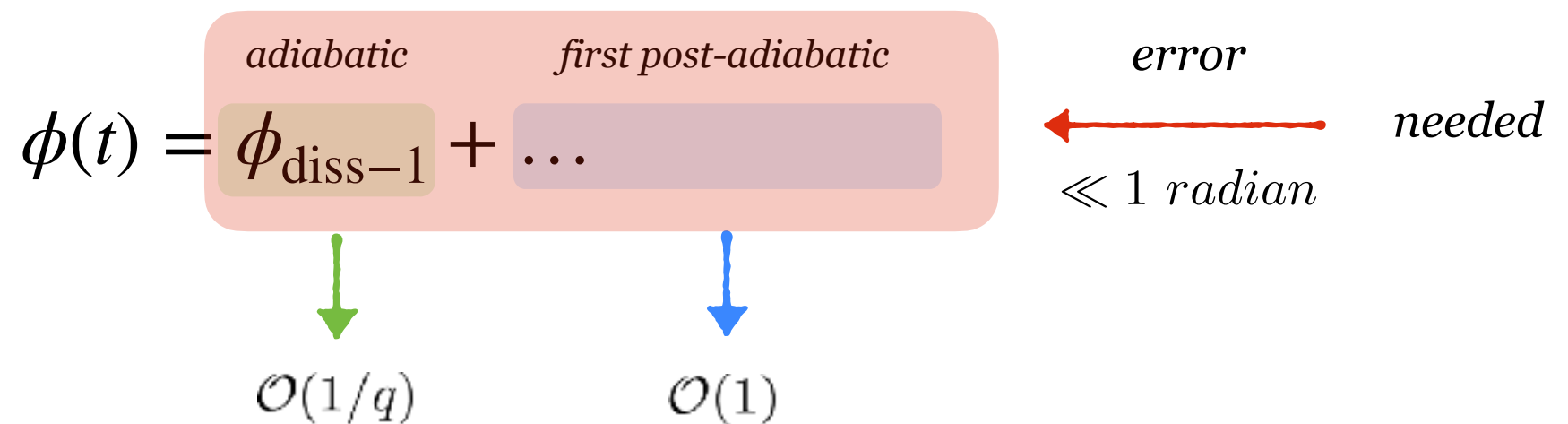
$$g_{\alpha\beta} = g_{\alpha\beta}^{(0)} + h_{\alpha\beta}$$
$$G_{\mu\nu} = T_{\mu\nu}^p = 8\pi m_p \int \frac{\delta^{(4)}(x - y_p(\lambda))}{\sqrt{-g}} \frac{dy_p^\alpha}{d\lambda} \frac{dy_p^\beta}{d\lambda} d\lambda$$

leading 
adiabatic

Regge-Wheeler-Zerilli
(Schwarzschild
background)

Teukolsky
(Kerr
background)

- The solution determines the phase evolution



The perturbation scheme

For the gravitational sector

$$h_{\alpha\beta} = h_{\alpha\beta}^{\text{pol}} + h_{\alpha\beta}^{\text{ax}}$$

$(-1)^\ell \leftarrow \rightarrow (-1)^{\ell+1}$

$$\mathbf{hT} = \sum_{\ell=0}^{\infty} \sum_{m=-\ell}^{\ell} \boxed{\mathcal{A}_{\ell m}^{(0)} \mathbf{a}_{\ell m}^{(0)} + \mathcal{A}_{\ell m}^{(1)} \mathbf{a}_{\ell m}^{(1)} + \mathcal{A}_{\ell m} \mathbf{a}_{\ell m} + \mathcal{B}_{\ell m}^{(0)} \mathbf{b}_{\ell m}^{(0)} + \mathcal{B}_{\ell m} \mathbf{b}_{\ell m}} + \boxed{\mathcal{Q}_{\ell m}^{(0)} \mathbf{c}_{\ell m}^{(0)} + \mathcal{Q}_{\ell m} \mathbf{c}_{\ell m}}$$

$$+ \boxed{\mathcal{D}_{\ell m} \mathbf{d}_{\ell m} + \mathcal{G}_{\ell m} \mathbf{g}_{\ell m} + \mathcal{F}_{\ell m} \mathbf{f}_{\ell m}}$$

$$\mathbf{b}_{\ell m} = \frac{n_\ell r}{\sqrt{2}} \begin{pmatrix} 0 & 0 & 0 & 0 \\ 0 & 0 & Y_{,\theta}^{\ell m} & Y_{,\phi}^{\ell m} \\ 0 & Y_{,\theta}^{\ell m} & 0 & 0 \\ 0 & Y_{,\phi}^{\ell m} & 0 & 0 \end{pmatrix}$$

- 7 **polar** components + 3 **axial** harmonics
- For a spherically symmetric background the 2 families decouple
- In vacuum GR using the Regge-Wheeler-Zerilli gauge the components reduce to 1 axial and 1 polar functions

Regge & Wheeler, PRD 108, 1063 (1957)
 Zerilli, PRD 2, 2141 (1970)

The wave equations

2 master equations for 2 perturbations

$$e^{-\lambda} = 1 - 2M/r$$
$$\Lambda = \ell(\ell + 1)/2 - 1$$

$$\frac{d^2 R_{\ell m}}{dr_\star^2} + \left[\omega^2 - e^{-\lambda} \left(\frac{\ell(\ell + 1)}{r^2} - \frac{6M}{r^3} \right) \right] R_{\ell m} = J_{\text{ax}}$$

info on the
orbital setup

Regge-Wheeler

$$\frac{d^2 Z_{\ell m}}{dr_\star^2} + \left[\omega^2 - \frac{18M^3 + 18M^2 r \Lambda + 6Mr^2 \Lambda^2 + 2r^3 \Lambda^2 (1 + \Lambda)}{r^3 (3M + r \Lambda)} \right] Z_{\ell m} = J_{\text{pol}}$$

Zerilli

- Perturbations are need to compute the GW fluxes...

$$\dot{E}_{\text{grav}}^\pm = \frac{1}{64\pi} \sum_{\ell=2}^{\infty} \sum_{m=-\ell}^{\ell} \frac{(\ell+2)!}{(\ell-2)!} (\omega^2 |Z_{\ell m}^\pm|^2 + 4|R_{\ell m}^\pm|^2)$$

- ... which drive the orbital evolution

$$\frac{dr(t)}{dt} = -\dot{E} \frac{dr}{dE_{\text{orb}}} \quad , \quad \frac{d\Phi(t)}{dt} = \frac{M^{1/2}}{r_p^{3/2}}$$

↑
orbital phase

orbital
radius



The wave equations

2 master equations for 2 perturbations

$$e^{-\lambda} = 1 - 2M/r$$
$$\Lambda = \ell(\ell + 1)/2 - 1$$

$$\frac{d^2 R_{\ell m}}{dr_*^2} + \left[\omega^2 - e^{-\lambda} \left(\frac{\ell(\ell + 1)}{r^2} - \frac{6M}{r^3} \right) \right] R_{\ell m} = J_{\text{ax}}$$

info on the
orbital setup

Regge-Wheeler

$$\frac{d^2 Z_{\ell m}}{dr_*^2} + \left[\omega^2 - \frac{18M^3 + 18M^2 r \Lambda + 6Mr^2 \Lambda^2 + 2r^3 \Lambda^2 (1 + \Lambda)}{r^3 (3M + r \Lambda)} \right] Z_{\ell m} = J_{\text{pol}}$$

Zerilli

- Perturbations are need to compute the GW fluxes...

$$\dot{E}_{\text{grav}}^{\pm} = \frac{1}{64\pi} \sum_{\ell=2}^{\infty} \sum_{m=-\ell}^{\ell} \frac{(\ell+2)!}{(\ell-2)!} (\omega^2 |Z_{\ell m}^{\pm}|^2 + 4|R_{\ell m}^{\pm}|^2)$$

- ... which drive the orbital evolution

$$\text{orbital radius} \quad \leftarrow \quad \frac{dr(t)}{dt} = -\dot{E} \frac{dr}{dE_{\text{orb}}} \quad , \quad \frac{d\Phi(t)}{dt} = \frac{M^{1/2}}{r_p^{3/2}}$$

↑
orbital phase

The wave equations

2 master equations for 2 perturbations

$$e^{-\lambda} = 1 - 2M/r$$
$$\Lambda = \ell(\ell + 1)/2 - 1$$

$$\frac{d^2 R_{\ell m}}{dr_*^2} + \left[\omega^2 - e^{-\lambda} \left(\frac{\ell(\ell + 1)}{r^2} - \frac{6M}{r^3} \right) \right] R_{\ell m} = J_{\text{ax}}$$

info on the orbital setup

Regge-Wheeler

$$\frac{d^2 Z_{\ell m}}{dr_*^2} + \left[\omega^2 - \frac{18M^3 + 18M^2 r \Lambda + 6Mr^2 \Lambda^2 + 2r^3 \Lambda^2 (1 + \Lambda)}{r^3 (3M + r \Lambda)} \right] Z_{\ell m} = J_{\text{pol}}$$

Zerilli

- Perturbations are need to compute the GW fluxes...

$$\dot{E}_{\text{grav}}^{\pm} = \frac{1}{64\pi} \sum_{\ell=2}^{\infty} \sum_{m=-\ell}^{\ell} \frac{(\ell+2)!}{(\ell-2)!} (\omega^2 |Z_{\ell m}^{\pm}|^2 + 4|R_{\ell m}^{\pm}|^2)$$

- ... which drive the orbital evolution

$$\text{orbital radius} \quad \leftarrow \quad \frac{dr(t)}{dt} = -\dot{E} \frac{dr}{dE_{\text{orb}}} \quad , \quad \frac{d\Phi(t)}{dt} = \frac{M^{1/2}}{r_p^{3/2}}$$

↑
orbital phase

How do we move on?

The landscape of calculations for asymmetric binaries is relatively virgin

- Analyses within **comparable-mass**, adding Newtonian terms to the orbital energy or the GW fluxes of the vacuum BBH baseline
- Inclusion of relativistic corrections to leading Newtonian terms show relevance of a fully relativistic descriptions

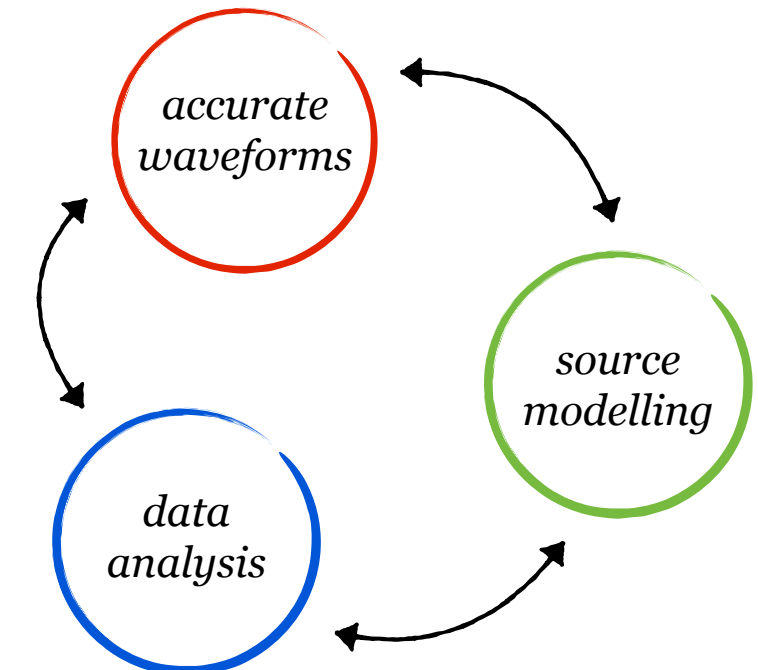
→ larger waveform dephasings

- lack of fully relativistic solutions able to describe BHs within a medium

→ need of background geometry to do our perturbative job

→ allows to study couplings between grav/fluid perturbations

→ impact on on QNMs, GW fluxes, particle motion



L. Sberna +, PRD 106, 064056 (2022)
L. Speri + 2207.10086
A. Toubiana +, PRL 126, 101105 (2021)
A. Coogan + PRD 105, 043009 (2022)
N. Speeney+ PRD 106, 044027 (2022)
...

The Background

The Einstein cluster prescription

V. Cardoso +, PRD Lett. 105, L061501, (2022)
V. Cardoso +, PRL 129, 241103, (2022)

- Reduces matter distribution to average anisotropic stress energy tensor

$$\langle T^{\mu\nu} \rangle = \frac{n}{m_p} \langle P^\mu P^\nu \rangle \longleftrightarrow T^\mu{}_\nu = \text{diag}(-\rho, 0, p_t, p_t)$$

A. Einstein, Annals Math. 40 (1939)

- Spherical symmetry

$$ds^2 = -a(r) dt^2 + \frac{dr^2}{1 - 2m(r)/r} + r^2 d\Omega^2$$

- Choose mass profile: we focused on DM rich environments

$$m(r) = M_{\text{BH}} + \frac{Mr^2}{(a_0 + r)^2} \left(1 - \frac{2M_{\text{BH}}}{r}\right)^2$$

Hernquist profile

L. Hernquist, The Astrroph. Journal 356 (1990)

- Generalized to any density profiles with radial dependence

E. Figueiredo, A.M. V. Cardoso, 2303.08183
Jusufi, arXiv:2202.00010
Igata et al, arXiv:2202.00202
Konoplya et al., The Astrroph. Journal 933 (2020)

The Background

- Solve the Einstein's fields equations sourced by the halo stress-energy tensor

$$\rho(r) = \frac{2M(a_0 + 2M_{\text{BH}})(1 - 2M_{\text{BH}}/r)}{4\pi r(r + a_0)^3}$$

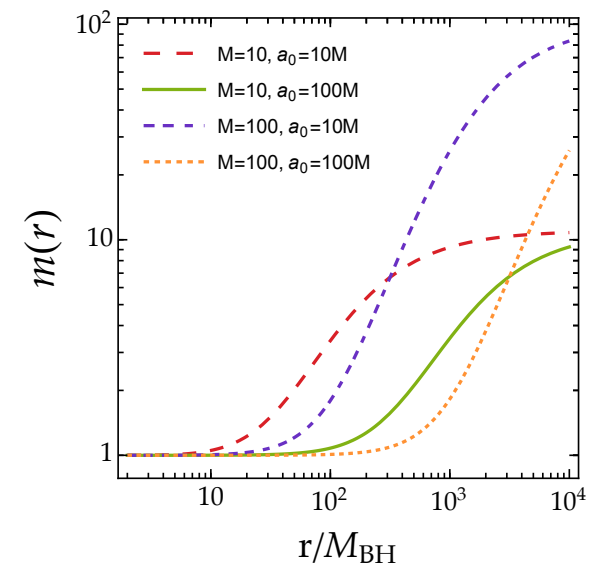
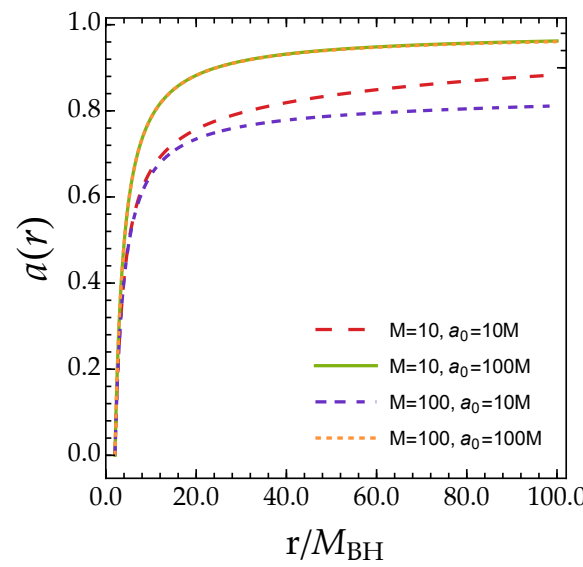
$$a(r) = \left(1 - \frac{2M_{\text{BH}}}{r}\right) e^{\Gamma}$$

$$\begin{aligned} \Gamma &= -\pi \sqrt{\frac{M}{\xi}} + 2\sqrt{\frac{M}{\xi}} \arctan \frac{r + a_0 - M}{\sqrt{M\xi}} \\ \xi &= 2a_0 - M + 4M_{\text{BH}} \end{aligned}$$

- To mimic galaxy observations $a_0 \gtrsim 10^4 M$  $M_{\text{BH}} \ll M \ll a_0$

- Asymptotically flat

- Horizon at $r = 2M_{\text{BH}}$



The Background

- Solve the Einstein's fields equations sourced by the halo stress-energy tensor

$$\rho(r) = \frac{2M(a_0 + 2M_{\text{BH}})(1 - 2M_{\text{BH}}/r)}{4\pi r(r + a_0)^3}$$

$$a(r) = \left(1 - \frac{2M_{\text{BH}}}{r}\right) e^{\Gamma}$$

$$e^{\Gamma}$$

$$\Gamma = -\pi \sqrt{\frac{M}{\xi}} + 2\sqrt{\frac{M}{\xi}} \arctan \frac{r + a_0 - M}{\sqrt{M\xi}}$$

$$\xi = 2a_0 - M + 4M_{\text{BH}}$$

$$1 - 2M/a_0$$

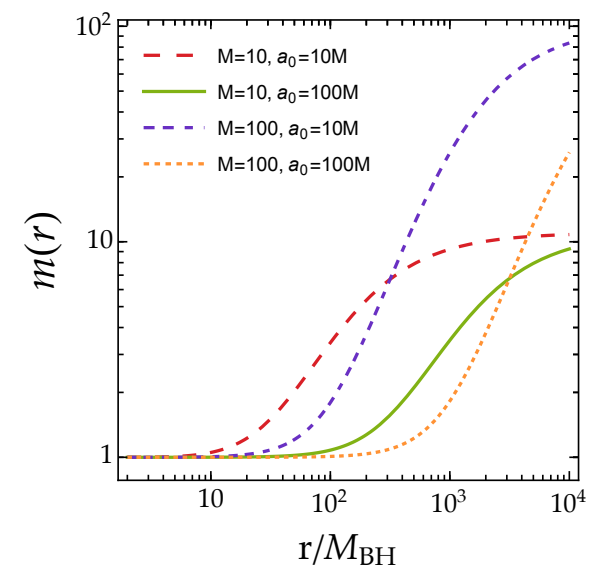
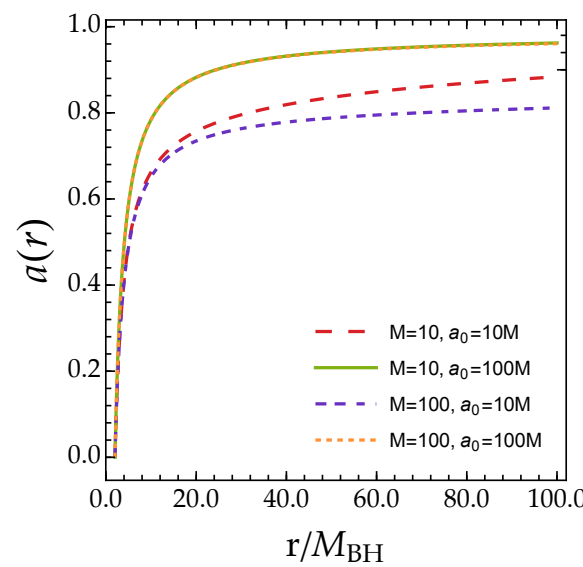
Redshift factor

- To mimic galaxy observations

$$a_0 \gtrsim 10^4 M \longrightarrow M_{\text{BH}} \ll M \ll a_0$$

- Asymptotically flat

- Horizon at $r = 2M_{\text{BH}}$



Geodesics

Generic halo configuration affects the orbital properties of massive and massless particles

$$r_{\text{LR}} \simeq 3M_{\text{BH}} \left(1 + \frac{MM_{\text{BH}}}{a_0^2} \right) \quad \longrightarrow \quad M_{\text{BH}}\Omega_{\text{LR}} \simeq \frac{1}{3\sqrt{3}} \left(1 - \frac{M}{a_0} + \frac{M(M + 18M_{\text{BH}})}{6a_0^2} \right)$$

$$r_{\text{ISCO}} \simeq 6M_{\text{BH}} \left(1 - \frac{32MM_{\text{BH}}}{a_0^2} \right) \quad \longrightarrow \quad M_{\text{BH}}\Omega_{\text{ISCO}} \simeq \frac{1}{6\sqrt{6}} \left(1 - \frac{M}{a_0} + \frac{M(M + 396M_{\text{BH}})}{6a_0^2} \right)$$

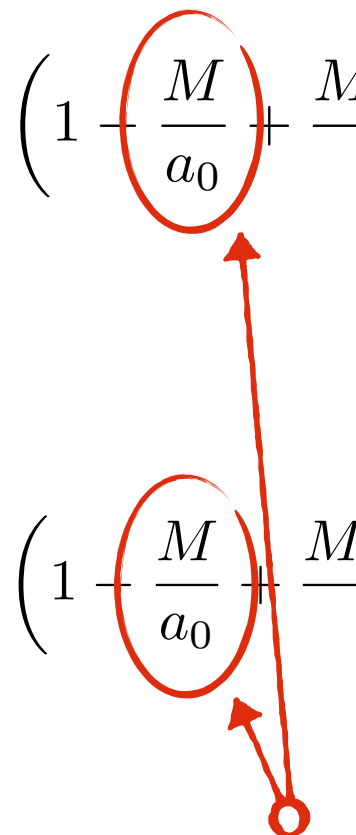
- At the leading order the halo only redshifts the dynamics
- BH shadow gets correction of the order $M^2/a_0^2 \lesssim 10^{-8}$ (light-ring tests are safe)

Geodesics

Generic halo configuration affects the orbital properties of massive and massless particles

$$r_{\text{LR}} \simeq 3M_{\text{BH}} \left(1 + \frac{MM_{\text{BH}}}{a_0^2} \right) \quad \longrightarrow \quad M_{\text{BH}}\Omega_{\text{LR}} \simeq \frac{1}{3\sqrt{3}} \left(1 - \frac{M}{a_0} + \frac{M(M + 18M_{\text{BH}})}{6a_0^2} \right)$$

$$r_{\text{ISCO}} \simeq 6M_{\text{BH}} \left(1 - \frac{32MM_{\text{BH}}}{a_0^2} \right) \quad \longrightarrow \quad M_{\text{BH}}\Omega_{\text{ISCO}} \simeq \frac{1}{6\sqrt{6}} \left(1 - \frac{M}{a_0} + \frac{M(M + 396M_{\text{BH}})}{6a_0^2} \right)$$

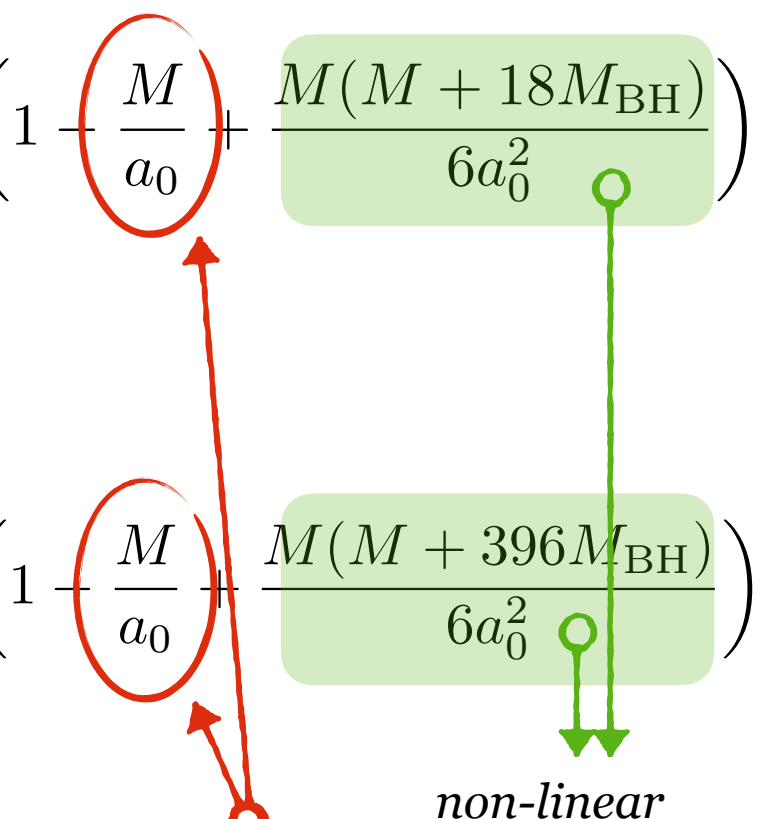


- At the leading order the halo only redshifts the dynamics
- BH shadows gets correction of the order $M^2/a_0^2 \lesssim 10^{-8}$ (light-ring tests are safe)

Geodesics

Generic halo configuration affects the orbital properties of massive and massless particles

$$r_{\text{LR}} \simeq 3M_{\text{BH}} \left(1 + \frac{MM_{\text{BH}}}{a_0^2} \right) \quad \xrightarrow{\text{green arrow}} \quad M_{\text{BH}}\Omega_{\text{LR}} \simeq \frac{1}{3\sqrt{3}} \left(1 - \frac{M}{a_0} + \frac{M(M + 18M_{\text{BH}})}{6a_0^2} \right)$$

$$r_{\text{ISCO}} \simeq 6M_{\text{BH}} \left(1 - \frac{32MM_{\text{BH}}}{a_0^2} \right) \quad \xrightarrow{\text{blue arrow}} \quad M_{\text{BH}}\Omega_{\text{ISCO}} \simeq \frac{1}{6\sqrt{6}} \left(1 - \frac{M}{a_0} + \frac{M(M + 396M_{\text{BH}})}{6a_0^2} \right)$$


Redshift factor

non-linear corrections

- At the leading order the halo only redshifts the dynamics
- BH shadows gets correction of the order $M^2/a_0^2 \lesssim 10^{-8}$ (light-ring tests are safe)

Dirty perturbations

EMRI (and more) evolving within environments

- Consider linear perturbations of a BH+halo background induced by the small secondary $\mathcal{G}_{\mu\nu} = 8\pi(T_{\mu\nu} + T_{\mu\nu}^p)$

grav-sector	fluid-sector
$g_{\alpha\beta} = g_{\alpha\beta}^{(0)} + h_{\alpha\beta}^{\text{ax}} + h_{\alpha\beta}^{\text{pol}}$	$u_\mu = u_\mu^0 + u_\mu^1 \quad \rho = \rho_0 + \rho_1$ $p_t = p_t^0 + p_t^1 \quad p_r = p_r^1$

- Decompose $h_{\alpha\beta}$ and (u_μ, p, ρ) in tensor, vector, scalar spherical harmonics

- e.g. for the pressure field

$$p_t^1(t, r, \theta, \phi) = \sum_{\ell=0}^{\infty} \sum_{m=-\ell}^{\ell} \delta p_{t,\ell m}(t, r) Y_{\ell m}(\theta, \phi)$$

- Go to the Fourier space, replace into the field's equation and solve ODEs

- For BH-halo configurations this ‘simple’ reduction works only partially
 - We have extra equations for matter quantities

BH & halo: axial modes

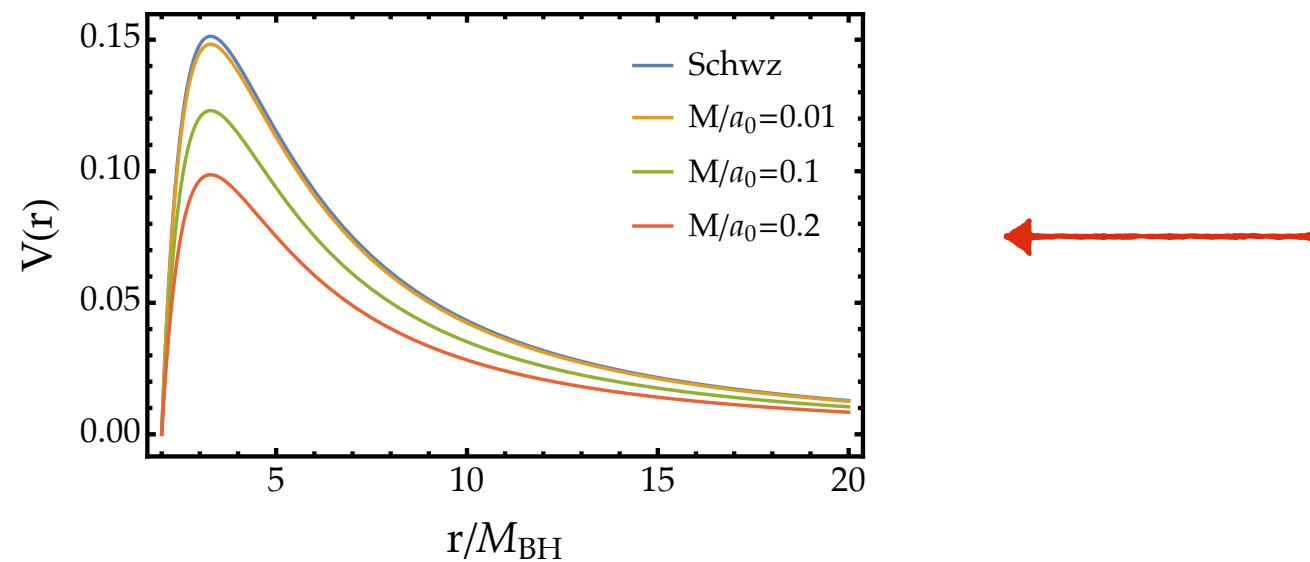
How does the halo change the axial perturbations of the BH?

- *Same functional form but...*

$$\frac{d^2 R_{\ell m}}{dr_*^2} + [\omega^2 - V^{\text{ax}}] R_{\ell m} = J_{\text{ax}}$$

$$V^{\text{ax}} = \frac{a(r)}{r^2} \left[\ell(\ell+1) - \frac{6m(r)}{r} + m'(r) \right]$$

- *Homogenous and in-homogenous problems provide the set up to study QNM and EMRI dynamics*



*Change in the scattering potential
due to the halo compactness*

- *The halo affects the structure of the potential, as well the boundary conditions of the wave propagation at the horizon and at infinity*
- *axial modes are not couple to fluid perturbations*

BH & halo: axial modes

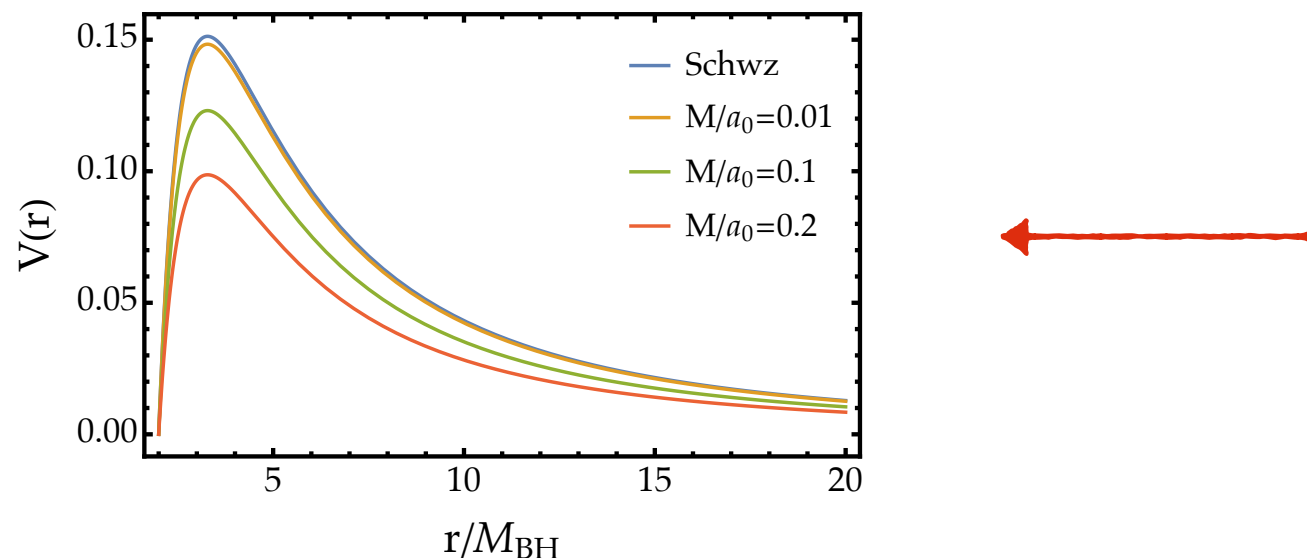
How does the halo change the axial perturbations of the BH?

- *Same functional form but...*

$$\frac{d^2 R_{\ell m}}{dr_*^2} + [\omega^2 - V^{\text{ax}}] R_{\ell m} = J_{\text{ax}}$$

$$V^{\text{ax}} = \frac{a(r)}{r^2} \left[\ell(\ell+1) - \frac{6m(r)}{r} + m'(r) \right]$$

- *Homogenous and in-homogenous problems provide the set up to study QNM and EMRI dynamics*



*Change in the scattering potential
due to the halo compactness*

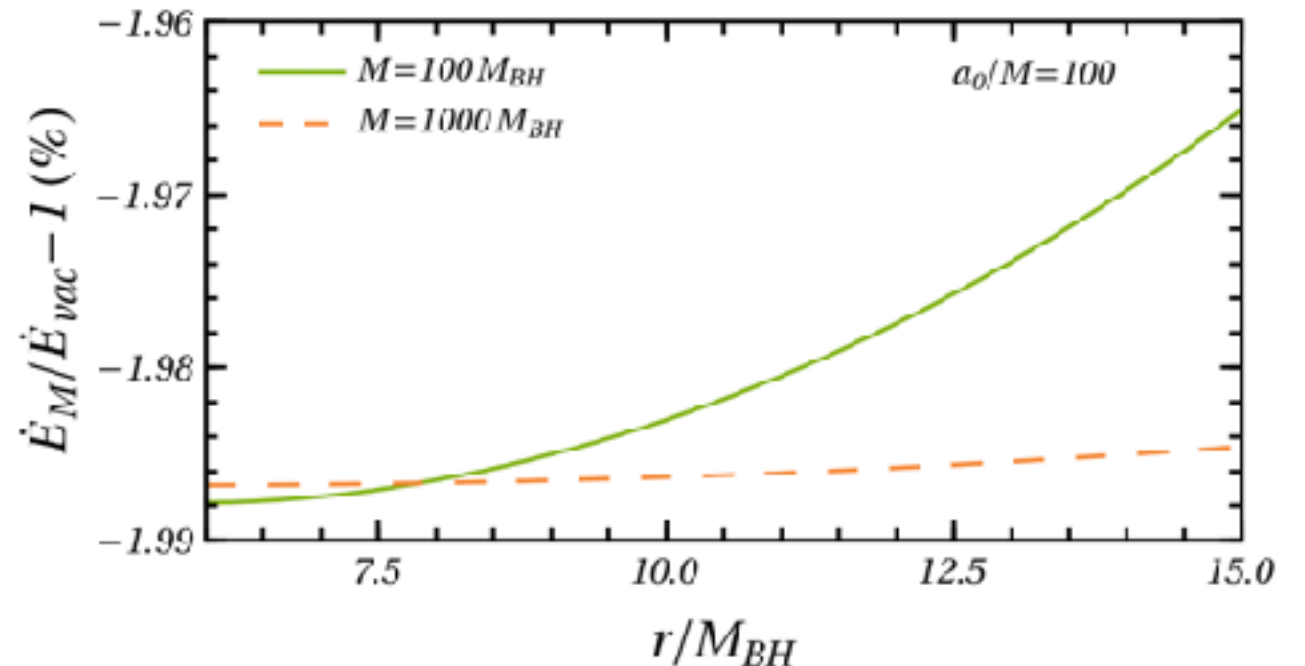
- *The halo affects the structure of the potential, as well the boundary conditions of the wave propagation at the horizon and at infinity*
- *axial modes are not couple to fluid perturbations*

BH & halo EMRI: axial modes

The halo properties affect the GW emission and hence the EMRI inspiral evolution (already) at adiabatic level

V.Cardoso +, PRD Lett. 105, L061501, (2022)

*Relative change in
the axial flux v.s.
vacuum*



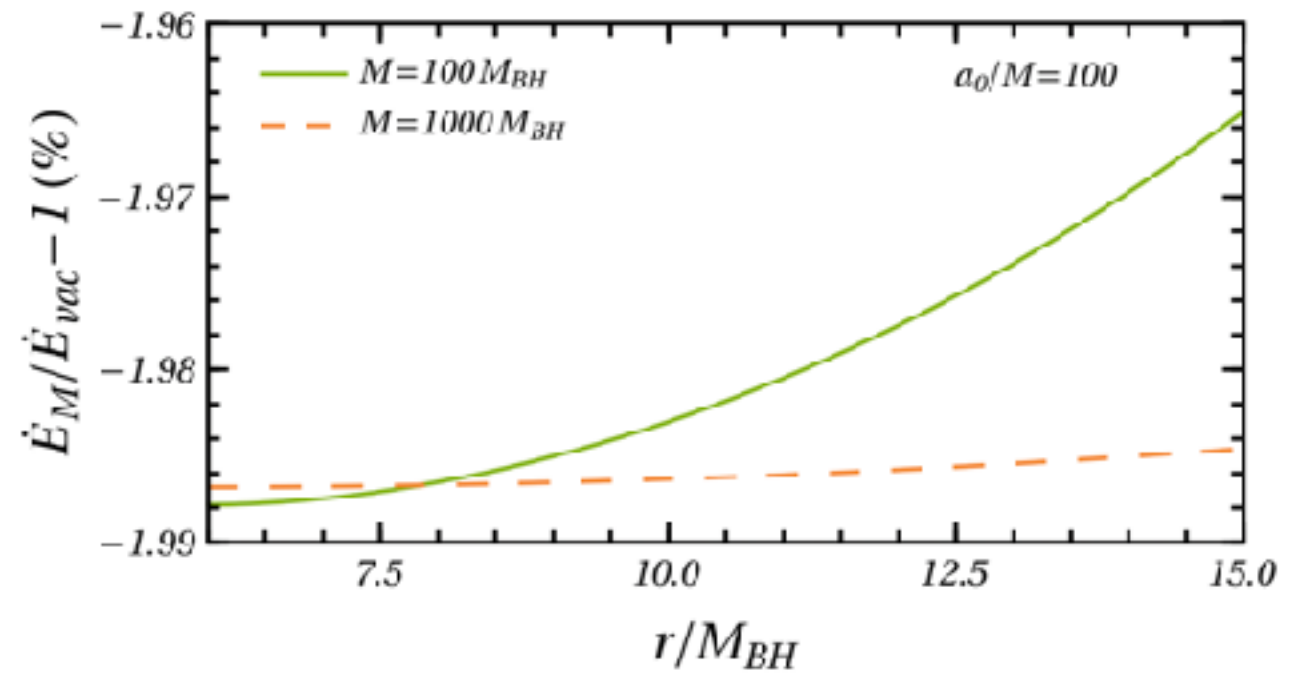
- *The difference with vacuum grows with M*
- *Suppression as M/a_0 decreases*
- *Difference << 1% as $M/a_0 \sim 10^{-3}$*

BH & halo EMRI: axial modes

The halo properties affect the GW emission and hence the EMRI inspiral evolution (already) at adiabatic level

V.Cardoso +, PRD Lett. 105, L061501, (2022)

*Relative change in
the axial flux v.s.
vacuum*



- The difference with vacuum grows with M
- Suppression as M/a_0 decreases
- Difference $\ll 1\%$ as $M/a_0 \sim 10^{-3}$

1 year
observation

before
the plunge

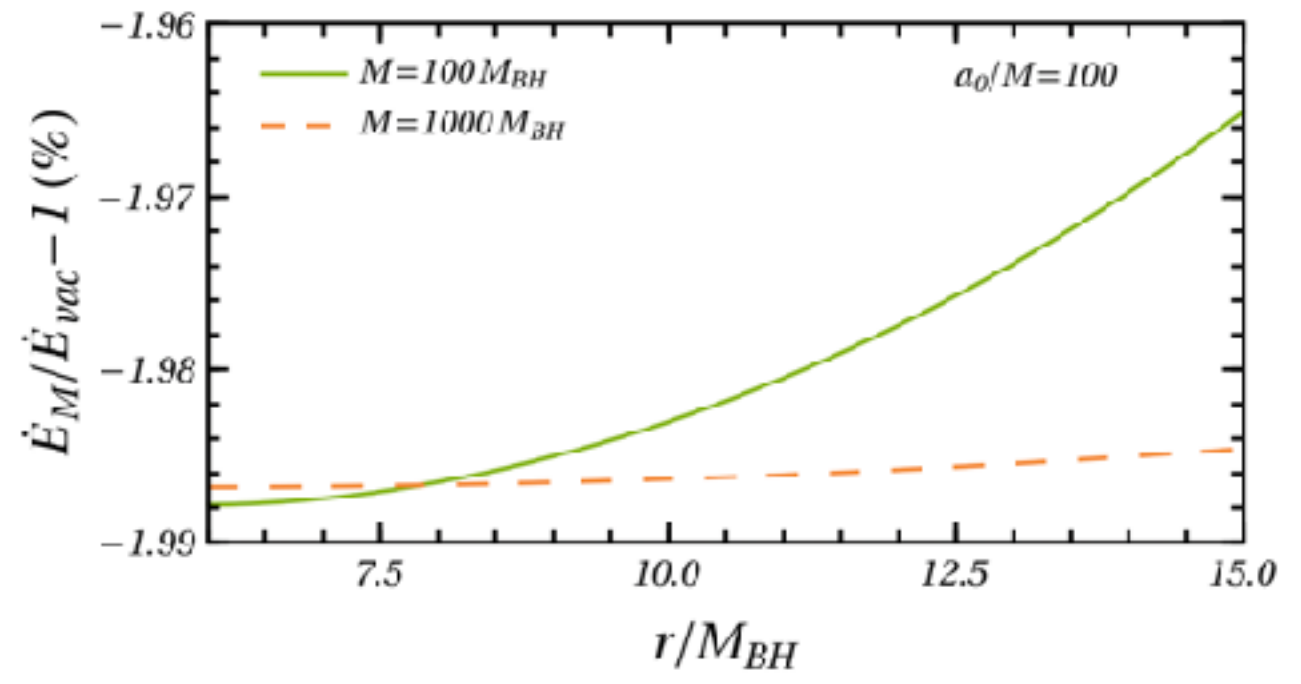
~ 500 radians

BH & halo EMRI: axial modes

The halo properties affect the GW emission and hence the EMRI inspiral evolution (already) at adiabatic level

V.Cardoso +, PRD Lett. 105, L061501, (2022)

*Relative change in
the axial flux v.s.
vacuum*



- The difference with vacuum grows with M
- Suppression as M/a_0 decreases
- Difference $<< 1\%$ as $M/a_0 \sim 10^{-3}$

look promising
but...

The redshift strikes back

Series expansion for low compactness $M/a_0 \ll 1$

$$V^{\text{ax}} \approx \left(1 - \frac{2M}{a_0}\right) V_{\text{Schw}}^{\text{ax}}$$

$$J_{\ell m}^{\text{ax}} \approx \mu \left(1 - \frac{3M}{a_0}\right) J_{\ell m}^{\text{ax,Schw}}$$

$$\frac{dr}{dr_\star} \approx \left(1 - \frac{M}{a_0}\right) \frac{dr}{dr_{\star,\text{Schw}}}$$

$$\frac{d^2 R_{\ell m}}{dr_{\star,\text{Schw}}^2} + \left[\left[\omega \left(1 + \frac{M}{a_0}\right) \right]^2 - V_{\text{Schw}}^{\text{ax}} \right] R_{\ell m} = \mu \left(1 - \frac{M}{a_0}\right) J_{\text{ax,Schw}}$$

The redshift strikes back

Series expansion for low compactness $M/a_0 \ll 1$

$$V^{\text{ax}} \approx \left(1 - \frac{2M}{a_0}\right) V_{\text{Schw}}^{\text{ax}}$$

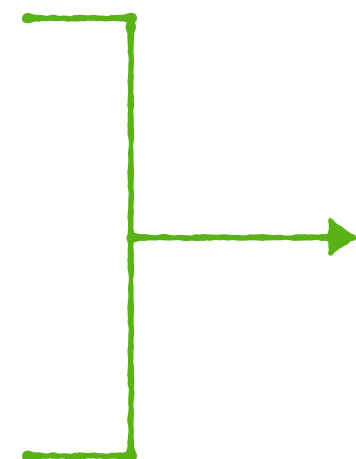
$$J_{\ell m}^{\text{ax}} \approx \mu \left(1 - \frac{3M}{a_0}\right) J_{\ell m}^{\text{ax,Schw}}$$

$$\frac{dr}{dr_{\star}} \approx \left(1 - \frac{M}{a_0}\right) \frac{dr}{dr_{\star,\text{Schw}}}$$



$$\frac{d^2 R_{\ell m}}{dr_{\star,\text{Schw}}^2} + \left[\left[\omega \left(1 + \frac{M}{a_0}\right) \right]^2 - V_{\text{Schw}}^{\text{ax}} \right] R_{\ell m} = \mu \left(1 - \frac{M}{a_0}\right) J_{\text{ax,Schw}}$$

$$\Omega_p \rightarrow \tilde{\Omega}_p = \Omega_p \left(1 - \frac{M}{a_0}\right)$$



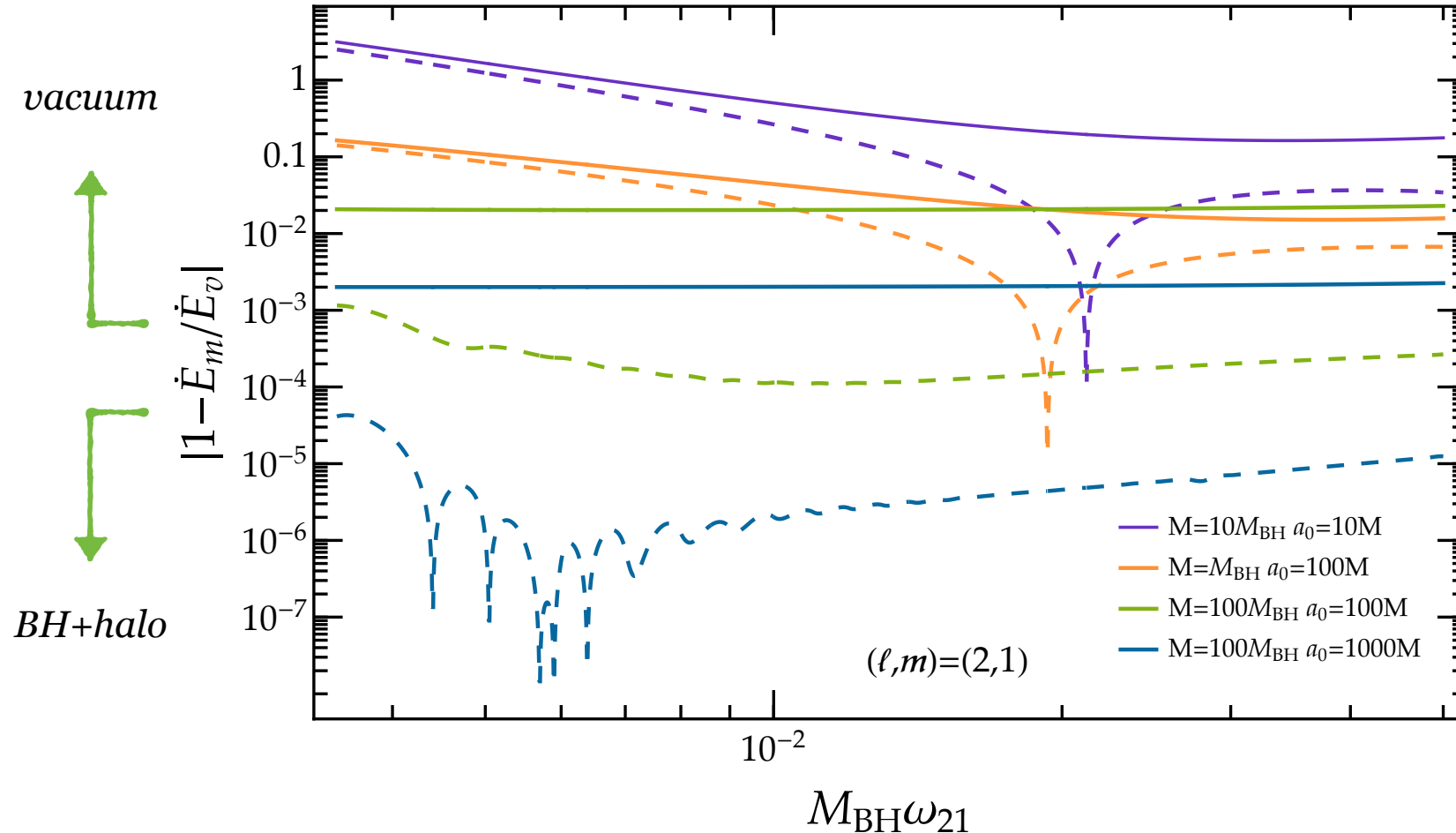
$$\mu \rightarrow \tilde{\mu} = \mu \left(1 + \frac{M}{a_0}\right)$$

*Equivalent to a vacuum solution
with rescaled parameters
(redshift of the BH mass scale)*

The redshift strikes back

(2,1) axial flux emitted by an EMRI on circular motion

- fluxes tend to be smaller in the presence of the halo

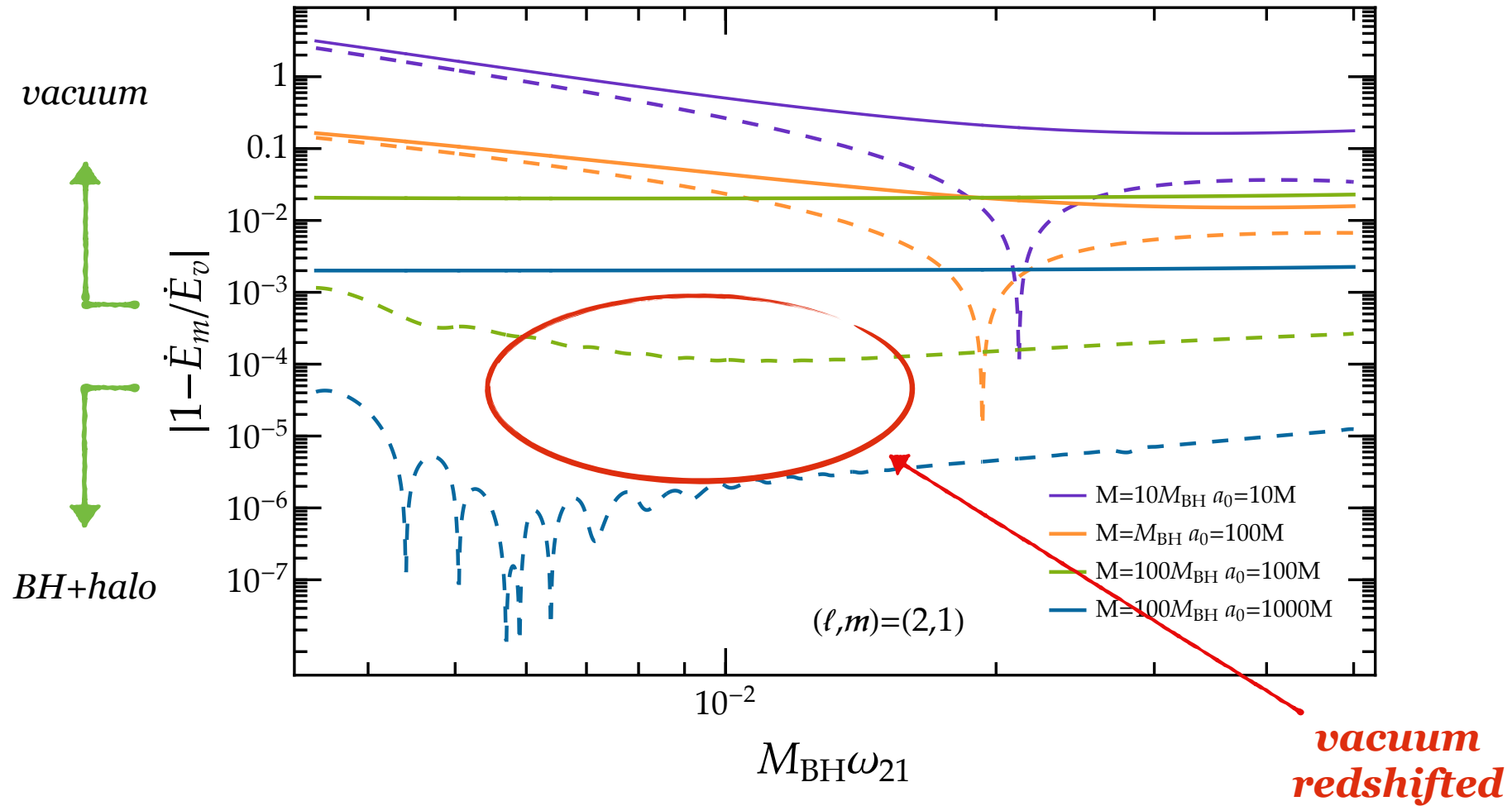


- Redshifted quantities drastically reduce the discrepancy for realistic halos
- Unless new effects pop up in the polar sector, the halo seems undetectable

The redshift strikes back

(2,1) axial flux emitted by an EMRI on circular motion

- fluxes tend to be smaller in the presence of the halo



- Redshifted quantities drastically reduce the discrepancy for realistic halos
- Unless new effects pop up in the polar sector, the halo seems undetectable

More general than it looks

Approach extended to generic density profiles

E. Figueiredo, A. M., V. Cardoso, 2303.08183

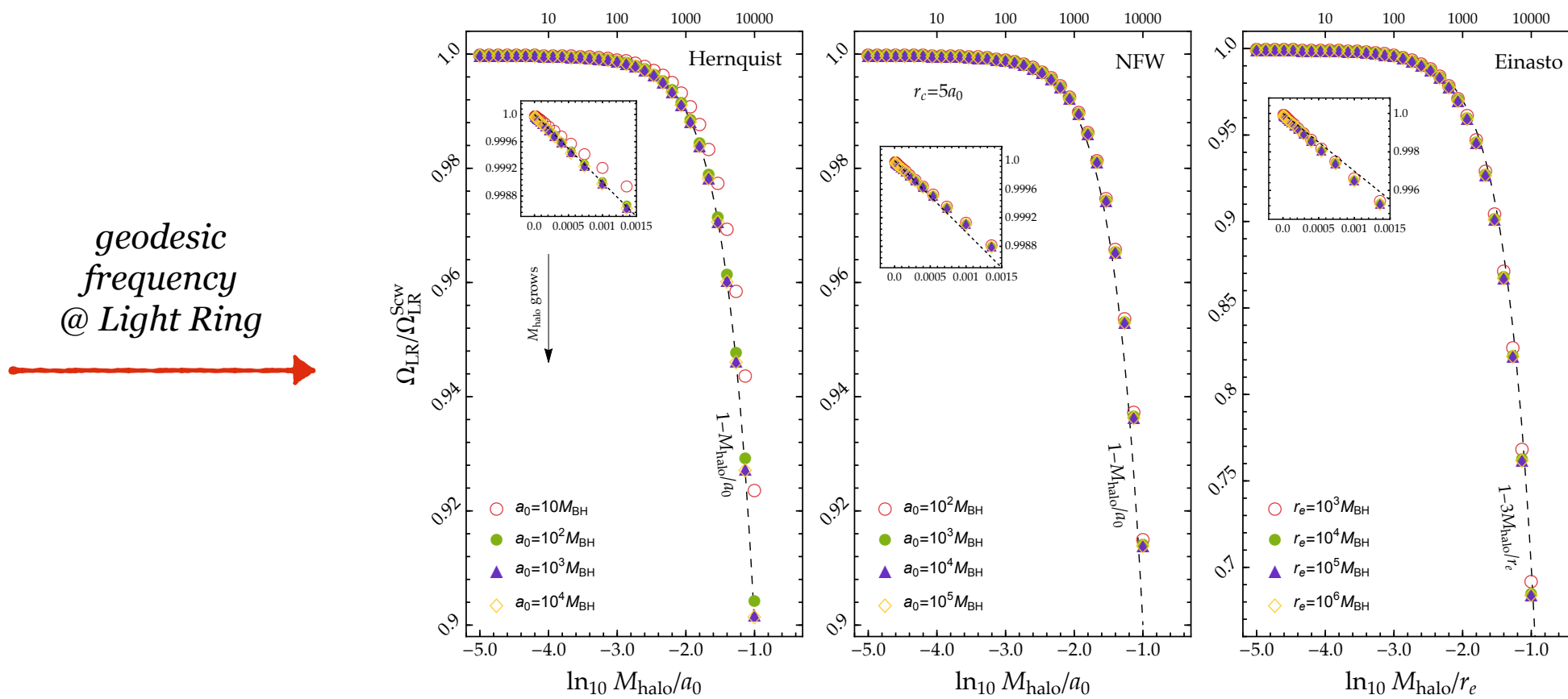
- Developed a fully numerical approach to treat any $\rho(r)$
- applied to new DM models

$$\rho(r) = \rho_0 (r/a_0)^{-\gamma} [1 + (r/a_0)^\alpha]^{(\gamma-\beta)/\alpha}$$

$$\rho(r) = \rho_e \exp \left\{ -d_n [(r/r_e)^{1/n} - 1] \right\}$$

Hernquist & Navarro-Frenk-White

Einasto



- Changes with respect to vacuum can be interpreted in terms of a “redshift” scaling

More general than it looks

Approach extended to generic density profiles

E. Figueiredo, A. M., V. Cardoso, 2303.08183

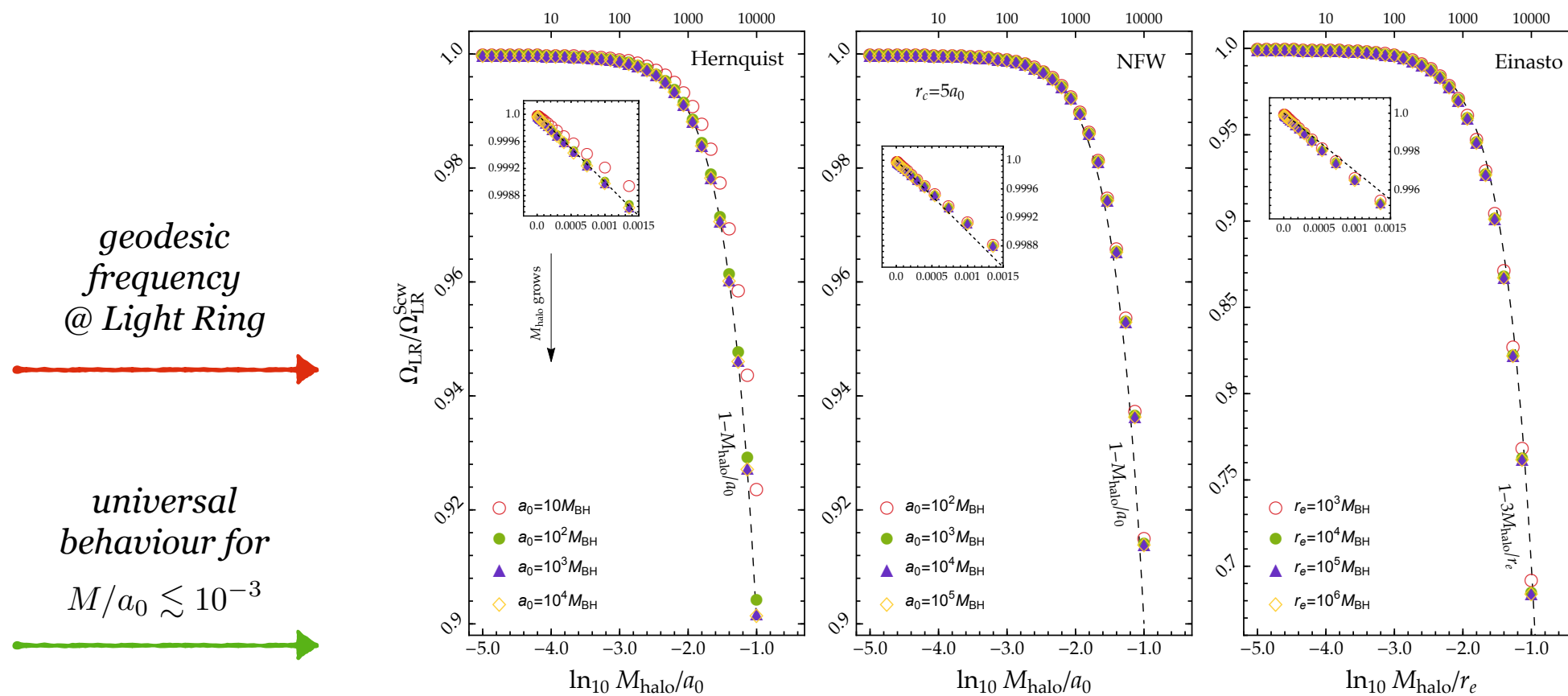
- Developed a fully numerical approach to treat any $\rho(r)$
- applied to new DM models

$$\rho(r) = \rho_0 (r/a_0)^{-\gamma} [1 + (r/a_0)^\alpha]^{(\gamma-\beta)/\alpha}$$

$$\rho(r) = \rho_e \exp \left\{ -d_n [(r/r_e)^{1/n} - 1] \right\}$$

Hernquist & Navarro-Frenk-White

Einasto

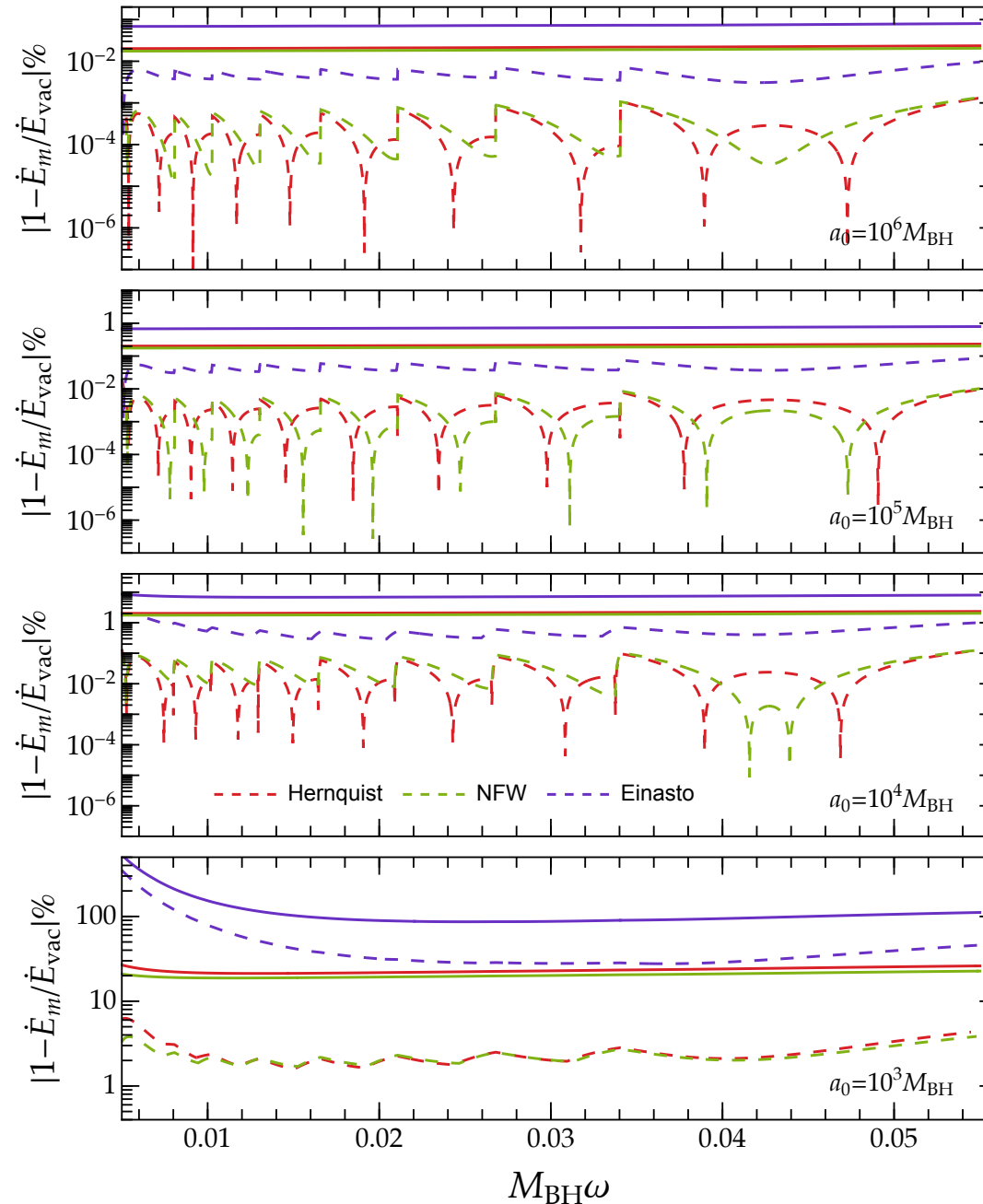


- Changes with respect to vacuum can be interpreted in terms of a “redshift” scaling

More general than it looks

Axial fluxes from EMRIs on circular orbits

E. Figueiredo, A.M., V. Cardoso, 2303.08183

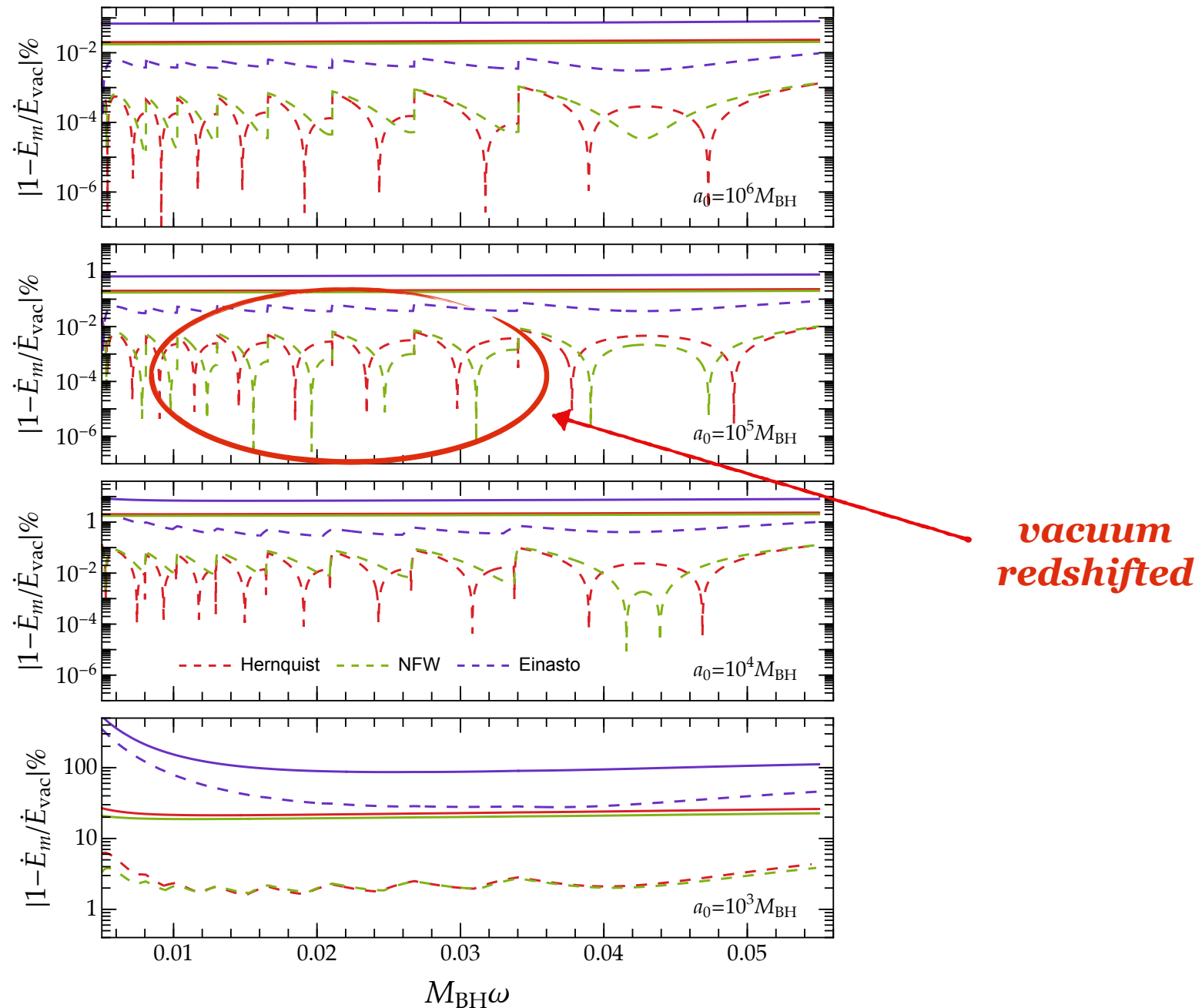


redshift (again) tends to suppress differences

More general than it looks

Axial fluxes from EMRIs on circular orbits

E. Figueiredo, A.M., V. Cardoso, 2303.08183



redshift (again) tends to suppress differences

BH & halo EMRI: polar modes

*Polar sector is more challenging due (more variables &) **couplings** between **matter** and **metric** components*

V. Cardoso.+, PRL 129, 241103, (2022)

- System of 5 coupled differential equations for $\vec{V} = (H_1, H_0, K, W, \delta\rho)$

$$\frac{d\vec{V}}{dr} = \mathbf{A}\vec{V} = \vec{S}$$

- The radial/tangential **speeds of sound** enter the modes

$$\begin{aligned}\delta p_{r,\ell m} &= c_{s_r}^2 \delta \rho_{\ell m} \\ \delta p_{t,\ell m} &= c_{s_t}^2 \delta \rho_{\ell m}\end{aligned}$$

$$M = 10M_{\text{BH}} \quad M/a_0 = 0.1$$

$$M \rightarrow 0$$

ℓ	m	\dot{E}_∞ (Finite Diff)	\dot{E}_∞ (FD _{inh})
2	2	1.7068011e-4	1.706(3)e-4
3	3	2.5489538e-5	2.547(3)e-5
4	4	4.7351723e-6	4.726(0)e-6

c_{s_r}	ℓ	m	\dot{E}_∞ (Finite Diff)	\dot{E}_∞ (FD _{inh})
	2	2	1.5903030e-4	1.579(3)e-4
	3	3	2.3162565e-5	2.314(0)e-5
	4	4	4.1593566e-6	4.167(0)e-6

c_{s_r}	ℓ	m	\dot{E}_∞ (Finite Diff)	\dot{E}_∞ (FD _{inh})
	2	2	1.6076861e-4	1.620(8)e-4
	3	3	2.3393697e-5	2.348(6)e-5
	4	4	4.0458012e-6	4.082(3)e-6

BH & halo EMRI: polar modes

Polar sector is more challenging due (more variables &) **couplings** between **matter** and **metric** components

V. Cardoso.+, PRL 129, 241103, (2022)

- System of 5 coupled differential equations for $\vec{V} = (H_1, H_0, K, W, \delta\rho)$

$$\frac{d\vec{V}}{dr} = \mathbf{A}\vec{V} = \vec{S}$$

- The radial/tangential **speeds of sound** enter the modes

$$\delta p_{r,\ell m} = c_{s_r}^2 \delta \rho_{\ell m}$$

$$\delta p_{t,\ell m} = c_{s_t}^2 \delta \rho_{\ell m}$$

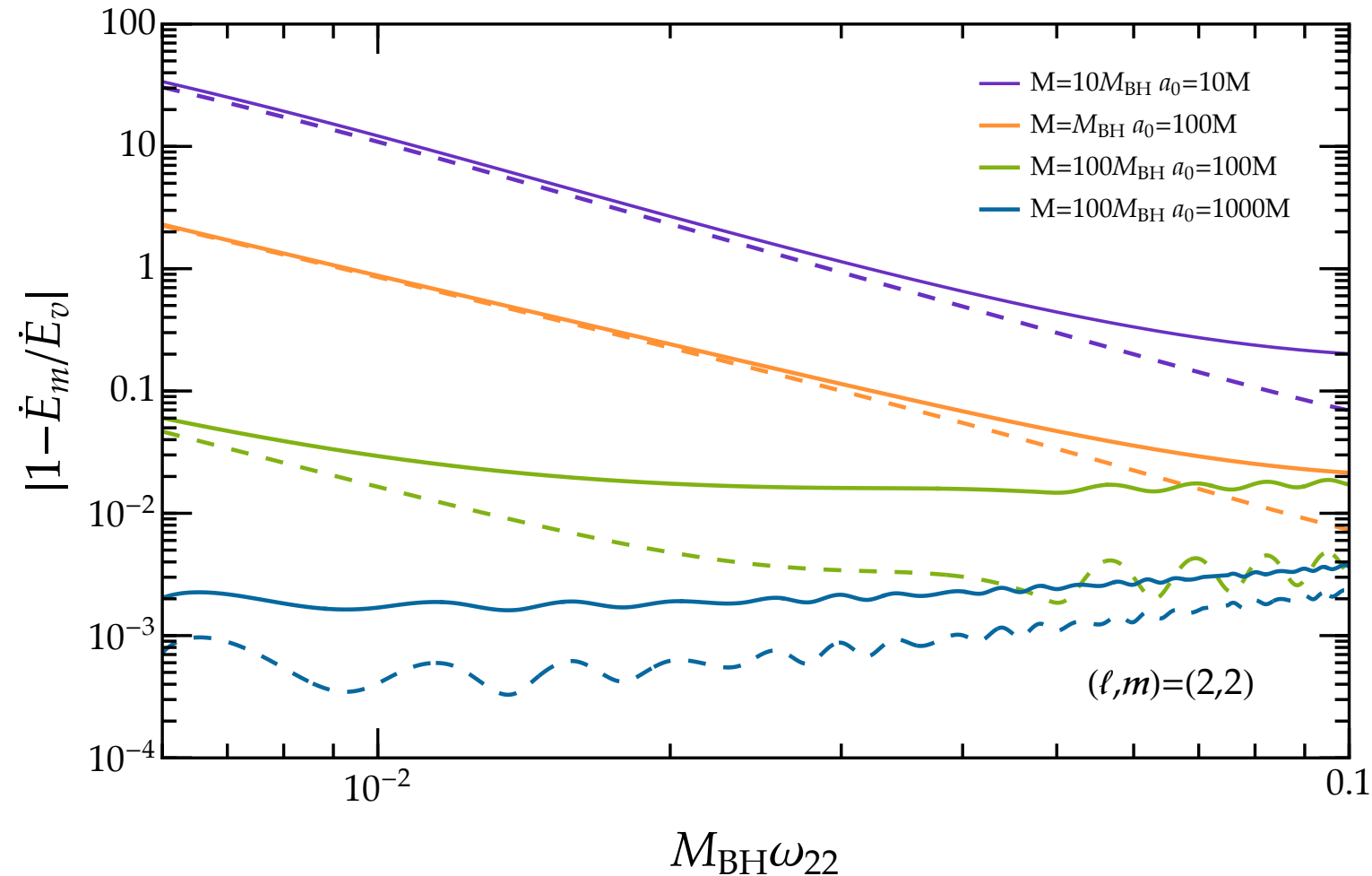
$M \rightarrow 0$		ℓ	m	\dot{E}_∞ (Finite Diff)	\dot{E}_∞ (FD _{inh})
2	2	1.7068011e-4		1.706(3)e-4	
3	3	2.5489538e-5		2.547(3)e-5	
4	4	4.7351723e-6		4.726(0)e-6	

c_{s_r}	$M = 10M_{\text{BH}}$		$M/a_0 = 0.1$	
	ℓ	m	\dot{E}_∞ (Finite Diff)	\dot{E}_∞ (FD _{inh})
2	2	2	1.5903030e-4	1.579(3)e-4
3	3	3	2.3162565e-5	2.314(0)e-5
4	4	4	4.1593566e-6	4.167(0)e-6

c_{s_r}	$M = 10M_{\text{BH}}$		$M/a_0 = 0.1$	
	ℓ	m	\dot{E}_∞ (Finite Diff)	\dot{E}_∞ (FD _{inh})
2	2	2	1.6076861e-4	1.620(8)e-4
3	3	3	2.3393697e-5	2.348(6)e-5
4	4	4	4.0458012e-6	4.082(3)e-6

BH & halo EMRI: polar modes

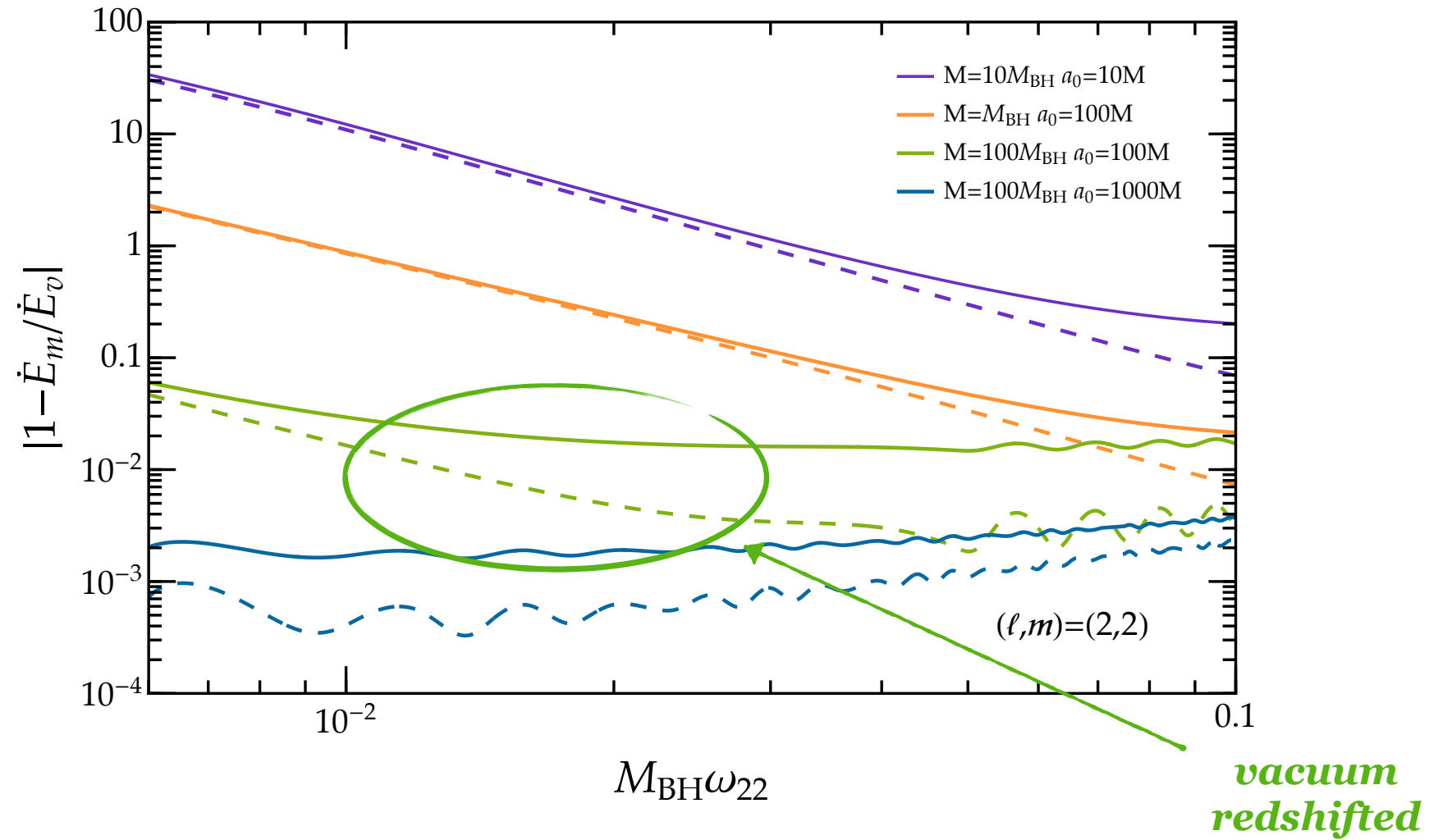
(2,2) polar flux emitted by an EMRI on circular motion



- Redshift rescaling not enough to take into account shift in the fluxes
- generation and propagation affected by deviations due to the coupling between polar modes and the fluid
- deviations seem “promising” in terms of detectability

BH & halo EMRI: polar modes

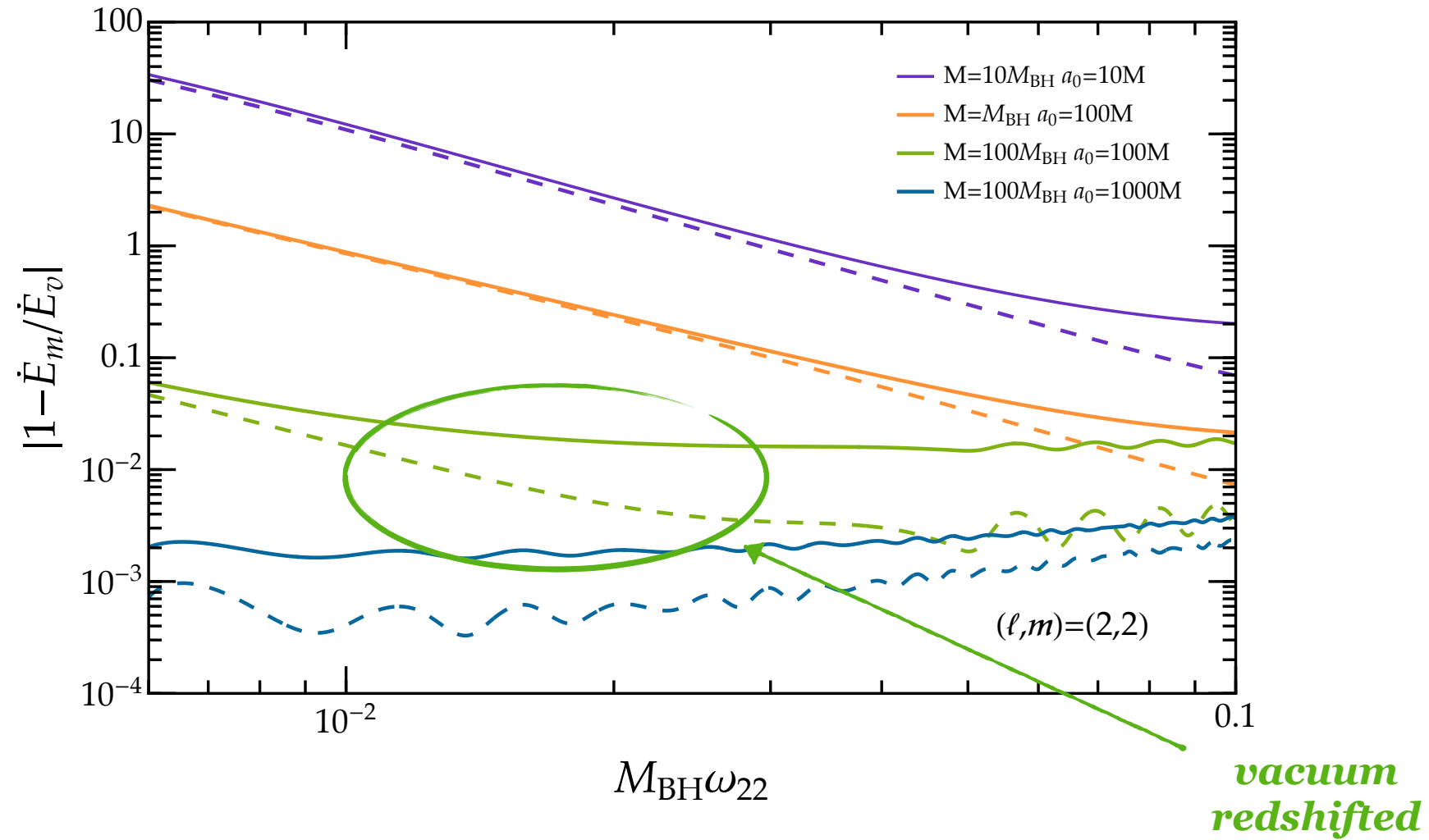
(2,2) polar flux emitted by an EMRI on circular motion



- Redshift rescaling not enough to take into account shift in the fluxes
- generation and propagation affected by deviations due to the coupling between polar modes and the fluid
- deviations seem “promising” in terms of detectability

BH & halo EMRI: polar modes

(2,2) polar flux emitted by an EMRI on circular motion



- Redshift rescaling not enough to take into account shift in the fluxes
- generation and propagation affected by deviations due to the coupling between polar modes and the fluid
- deviations seem “promising” in terms of detectability

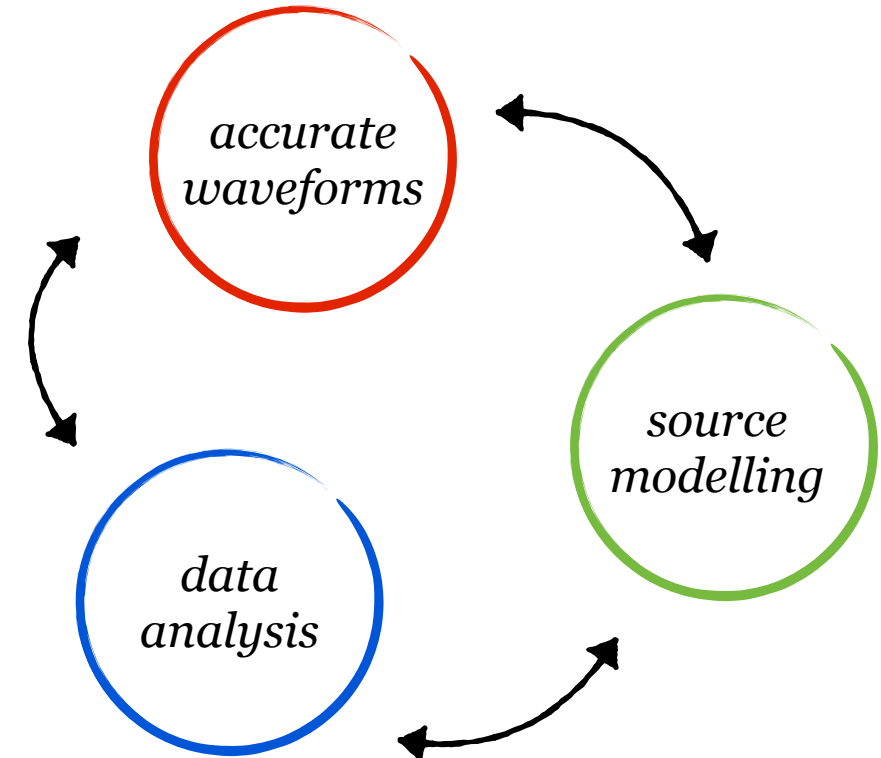


*new waveform
models to build*

EMRI in dirty backgrounds

First steps towards fully relativistic description

- *Ab-initio calculation of EMRI evolution with a non-vacuum BBH background*
- *Changes in the emitted gravitational wave fluxes due to the environment's properties*
- *GW propagation and generation can be strongly affected by coupling between polar modes and the fluid*



But

- *Rotating background for (more) realistic astrophysical BHs*
- *Waveform generation*
- *Detectability of halo parameters*
- *Degeneracy with beyond-GR modifications*

Back up

Wave equation (homogeneous)

Solving the homogeneous problem allows to study the dirty BH **Quasi-Normal-Mode** spectrum

$$\frac{d^2\psi_{\ell m}}{dr_*^2} + [\omega^2 - V]\psi_{\ell m} = 0$$

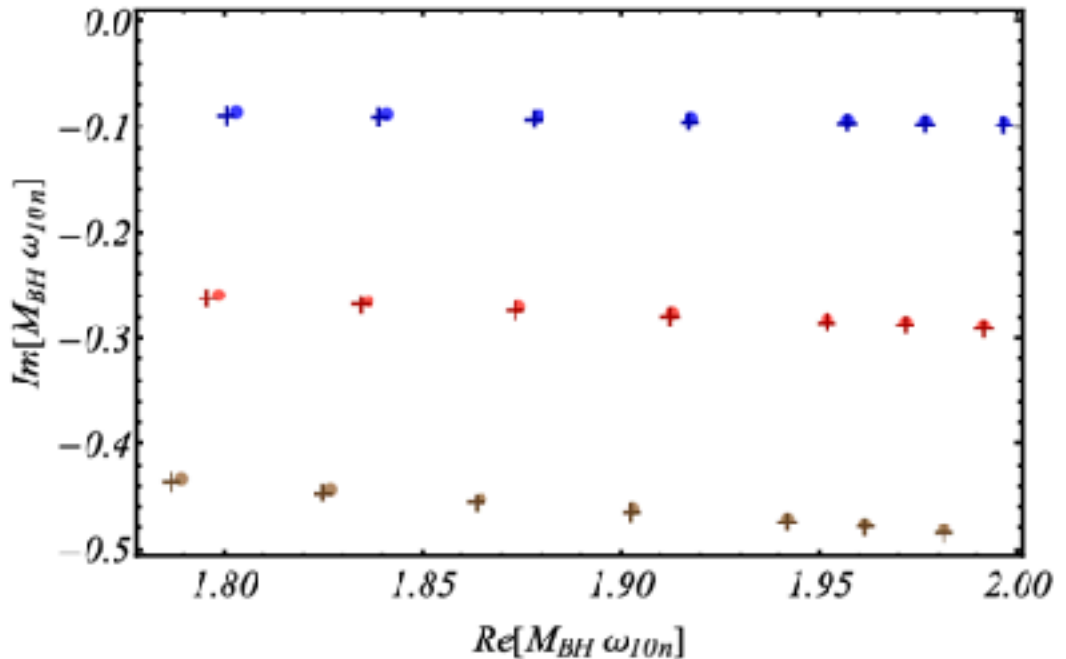
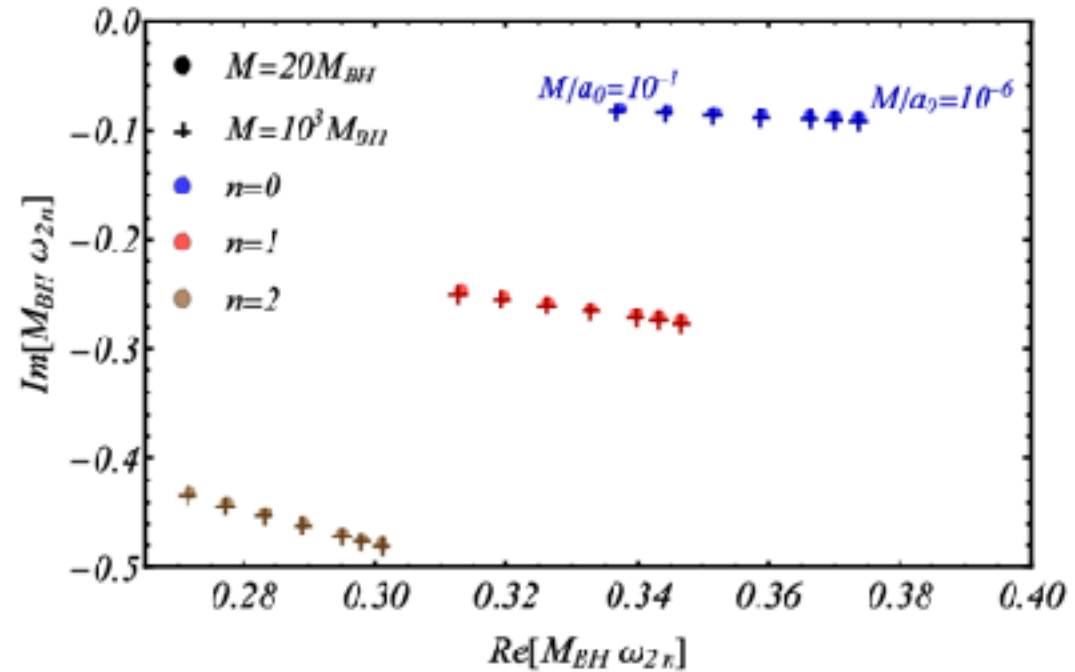
- Solve for the homogeneous part with suitably boundary conditions



- Find the system eigenvalues (the QNM frequencies) which render the two solutions dependent

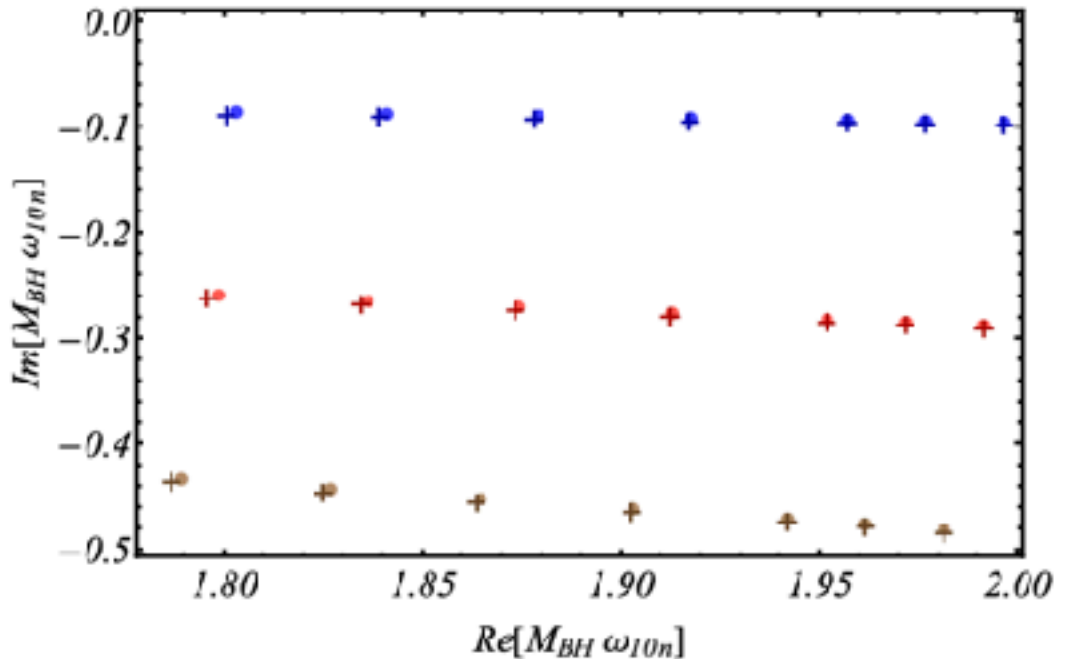
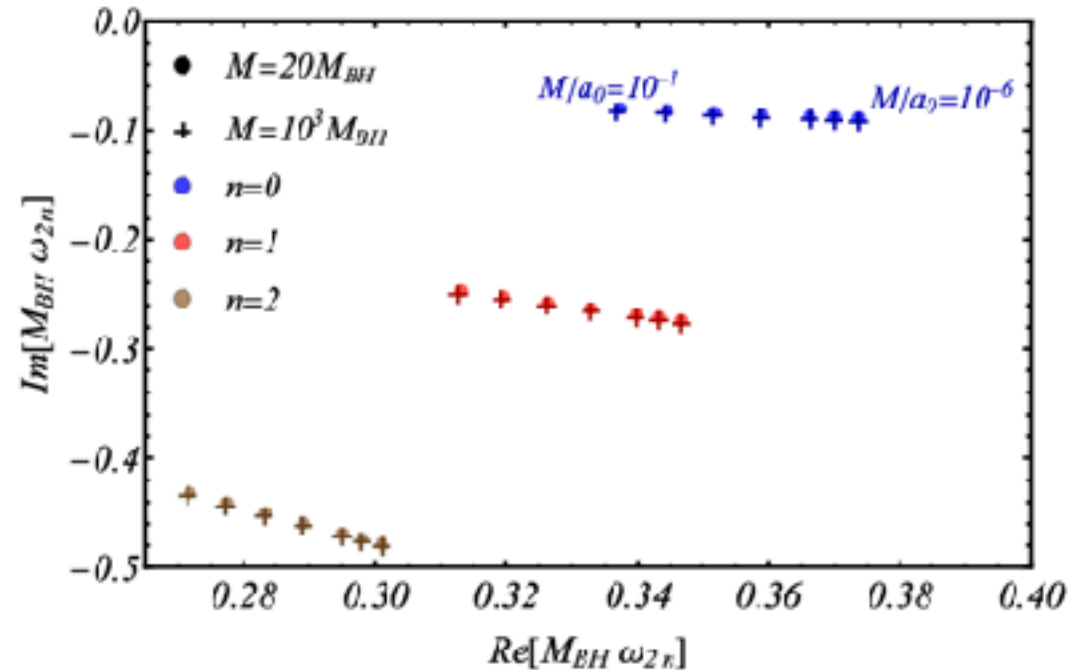
$$\psi_{\ell m}^{(-)} \psi_{\ell m}'^{(+)} - \psi_{\ell m}^{(+)} \psi_{\ell m}'^{(-)} = 0$$

Quasi Normal Modes



- Both real and imaginary part decrease as M/a_0 increases
- Very little dependence on M

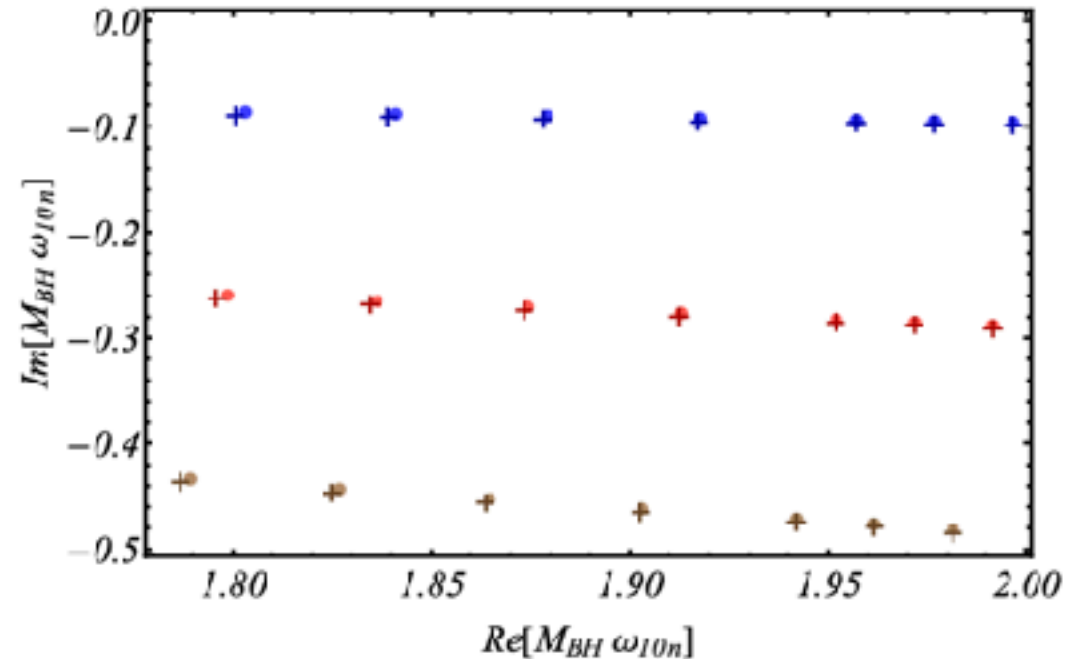
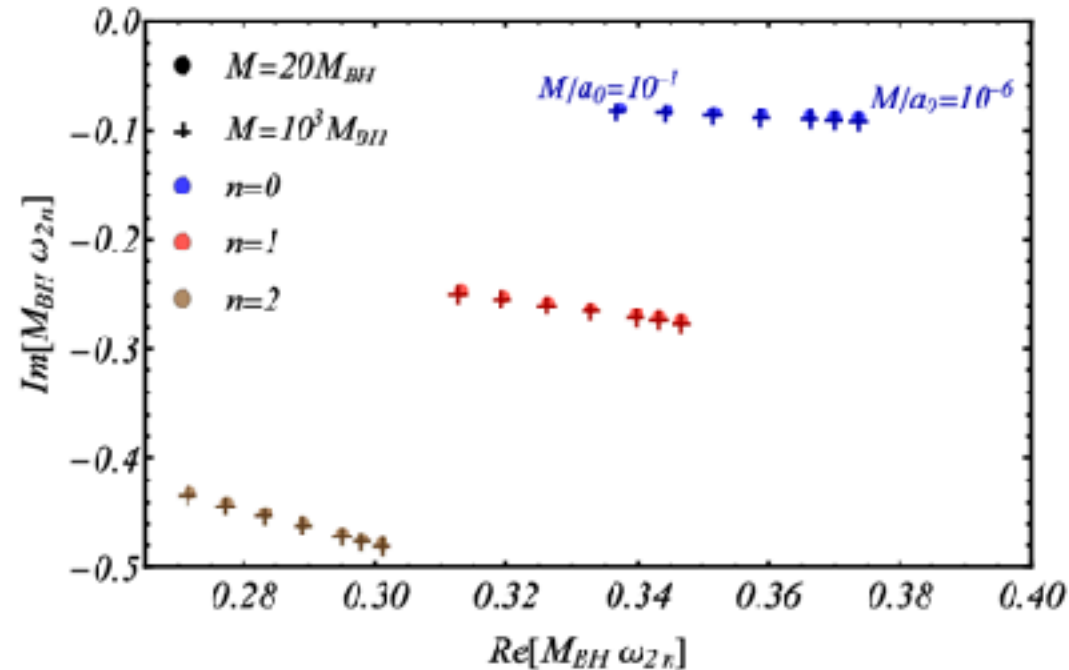
Quasi Normal Modes



- Both real and imaginary part decrease as M/a_0 increases
- Very little dependence on M

←
*redshift
effect*

Quasi Normal Modes



- Both real and imaginary part decrease as M/a_0 increases
- Very little dependence on M
- In the eikonal limit $\omega_{\text{QNM}} = \Omega_{\text{LR}}\ell - i(n + 1/2)|\lambda|$
- For small compactness

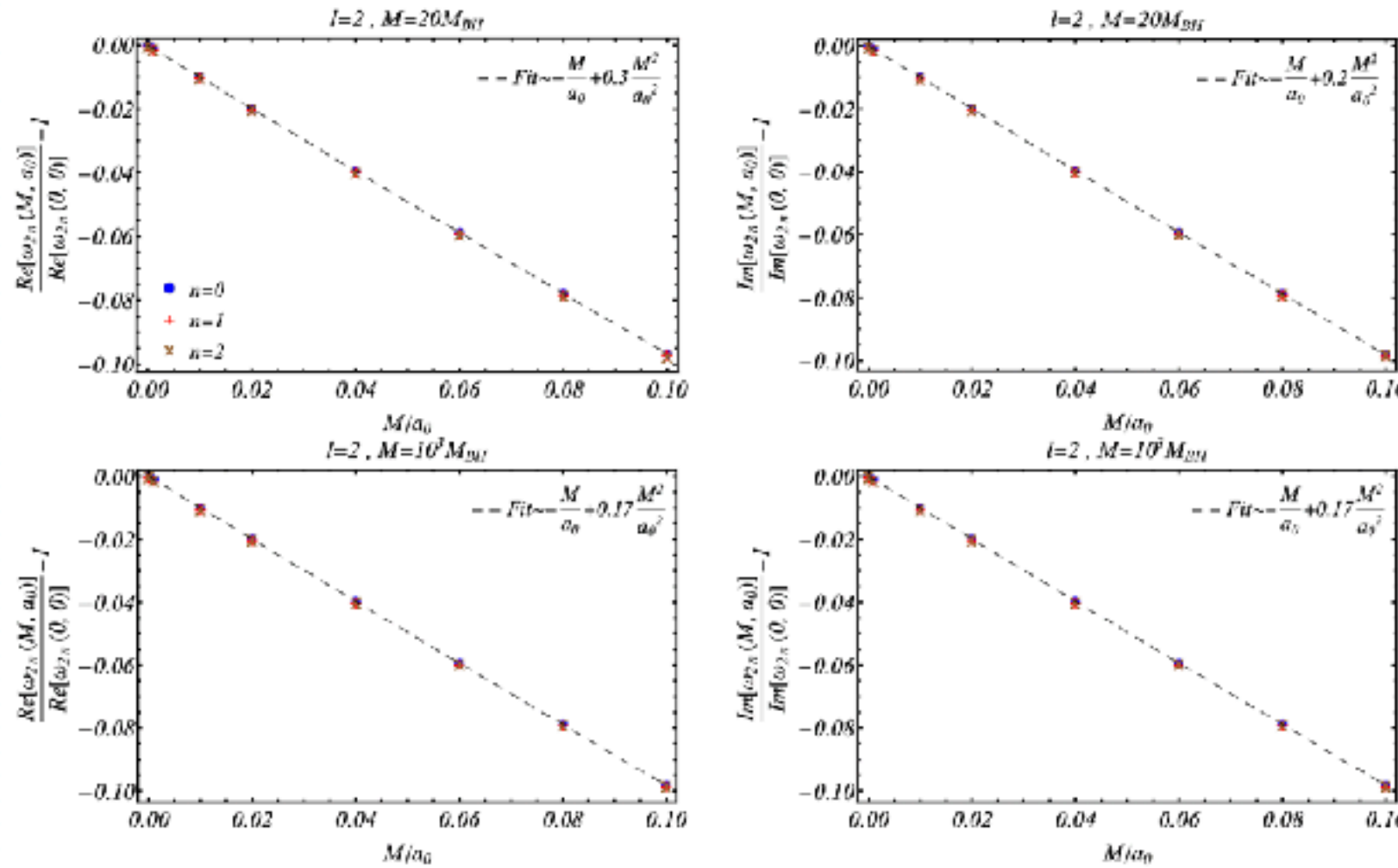
redshift
effect

$$\frac{\Omega_{\text{LR}}}{\Omega_{\text{LR}}^{\text{vac}}} \simeq 1 - \frac{M}{a_0} - 0.17 \frac{M^2}{a_0}$$

$$\frac{\lambda}{\lambda^{\text{vac}}} \simeq 1 - \frac{M}{a_0} - 0.17 \frac{M^2}{a_0}$$

Quasi Normal Modes

QNM behaviour as a function of the halo compactness



- The QNMs have a clear light-ring interpretation
- Linear and subdominant corrections agree with the analytic scaling of frequencies and damping times

Wave equation (inhomogeneous)

EMRI evolution by solving the full inhomogeneous problem

$$\frac{d^2\psi_{\ell m}}{dr_*^2} + [\omega^2 - V] \psi_{\ell m} = J_{\ell m}$$

- Solve for the homogeneous part with suitably boundary conditions



- Integrate over the source term for the full solution

$$\psi_{\ell m}^\pm \equiv \lim_{r_* \rightarrow \pm\infty} \psi_{\ell m}(r_*) = e^{\pm i\omega r_*} \int_{-\infty}^{\infty} \frac{\psi_{\ell m}^{(\mp)} J}{W} dr_*$$

- For circular orbits the integral greatly simplifies because of $\delta(r - r_p)$